Changes in the future summer Mediterranean climate: contribution of teleconnections and local factors.

Monika J. Barcikowska[1], Sarah B. Kapnick[2], Lakshmi Krishnamurty[3], Simone Russo[4], Annalisa Cherchi[5], Chris K. Folland[6,7,8]

[1]Environmental Defense Fund, New York City
[2]Geophysical Fluid Dynamics Laboratory, National Oceanic and Atmospheric Administration, 201 Forrestal Road, Princeton, NJ 08540, USA
[3]Princeton University, GFDL Princeton University Forrestal Campus, 201, Forrestal Road, Princeton, NJ 08542, USA
[4]European Commission, Joint Research Centre, Via Enrico Fermi, Ispra, Italy
[5]Fondazione Centro Euro-Mediterraneo sui Cambiamenti Climatici, and Istituto Nazionale di Geofisica e Vulcanologia, Bologna, Italy
[6]School of Environmental Sciences, University of East Anglia, Norwich, UK
[7]Department of Earth Sciences, University of Gothenburg, Sweden
[8]International Centre for Applied Climate Sciences, University of Southern Queensland, Australia

Abstract

The simulated regional future changes for the Mediterranean region in summer with a high resolution coupled model (CM2.5) suggest pronounced warming and drying over most parts of the region. However, the changes are distinctively less radical when compared with the CMIP5 multi-model ensemble. In addition, changes over the Southeast (off the coast area of the Balkans) and Central Europe indicate not only a very modest warming, compared to the CMIP5 projections, but also wetting tendencies. Our analysis highlights importance of a correctly projected magnitude of changes of the summer North Atlantic Oscillation and its regional impacts, which have the capacity to partly offset the anthropogenic warming and drying over the western and central Mediterranean. However, the difference of CM2.5 projections of future changes over previous-generation models indicates a possible role of other factors such as land surface-atmospheric interactions, which are a governing factor for thermal- and hydro-climate over Central and Southeastern Europe. De facto, CM2.5 incorporates a new and improved land model (LM3). The CM2.5 projections also indicate a maximum of warming (eastern Mediterranean land region) and drying (Asia Minor) over the eastern Mediterranean. In this specific region, the projected changes indicate a decreasing influence of atmospheric dynamics in maintaining the regional temperature and precipitation balance and instead an increasing influence of local surface temperature on the local surface atmospheric circulation.

1. Introduction

The climate of the Mediterranean region is primarily characterized by mild, wet winters and hot, dry summers. This climate zone is located between 30°-45°N, hence it is affected by the variability of the atmospheric circulation both in mid-latitudes and in the tropics. Moreover, the geomorphological characteristics of the

Mediterranean Sea region, including gulfs, peninsulas, islands, as well as the mountain ridges surrounding the basin, make the climate of this region distinctively complex.

The North Atlantic Oscillation and the East Atlantic pattern (e.g. Hurrell, 1995, Krichak et al. 2002, Barcikowska et al. 2017b) are the main manifestation of mid-latitudes influence for winter precipitation in the northern parts of the region. The summer expression of the NAO (SNAO, Folland et al. 2009, Linderholm et al., 2009, Blade et al. 2012), due to its northeastward-shifted location, affects the Mediterranean region, as well. The observations-based SNAO shows a northern lobe centered over southern Greenland and a southern lobe located close to the British Isles (Folland et al. 2009 and Blade et al. 2012). The positive SNAO phase yields a stronger meridional SLP gradient over the North Atlantic, an enhanced anticyclonic southern lobe with dry conditions over northwest Europe and rather wet conditions over the central Mediterranean. Several studies indicated an exisiting linkage between SNAO phases and the Atlantic Meridional Oscillation (Knight et al. 2006, Folland et al 2009, Linderholm and Folland 2017), which originates from both internal ocean variations (Knight et al. 2005, 2006, Delworth and Mann 2000; Enfield et al. 2001), and anthropogenic sources (Rotstayn and Lohman 2002; Mann and Emanuel 2006).However, current literature has not yet reached a full consensus on the spatial definition (fingerprint), origin and impacts of the SNAO. The results of observational analysis vary, depending on the observational dataset, the chosen period, the chosen summer months, and the analysis method (Barnston and Livezey, Hurrell and van Loon 1997, Hurrell and Folland 2002; Hurrell et al. 2003, 2009, Cassou et al. 2005, Folland 2009, Blade 2012). In fact, there is a strong sensitivity of the derived SNAO fingerprint to the chosen period (i.e., for shorter periods of about 30 years-length) with marked variations in the percentage of SLP variance explained over the selected domain (Blade et al 2012). These sensitivities support the notion that the derived component may stem from the combined effects of interannual to multi-decadal components, as highlighted by Folland et al. 2009 and Linderholm and Folland, 2017.

In summer, the northward shift of the Hadley cell reveals a connection between the hot and arid eastern part of the region and the Asian and African monsoons, as well as a possible connection between these two monsoons (Rodwell and Hoskins 1996, Ziv et al. 2004, Fontaine et al. 2011, Raicich et al. 2003, Rowell 2003). The regional summer climate features a seasonal minimum of the rainfall, persistent mid-level and upper–level subsidence and low-level northerlies (Raicich et al. 2003, Mariotti et al. 2002, Tyrlis et al. 2013) centered over the central-eastern part of the Mediterranean. The low-level northerlies are called Etesian winds (HMSO 1962; Metaxas 1977; Maheras 1980; Prezerakos 1984; Reddaway and Bigg 1996; Zecchetto and de Biasio 2007; Chronis et al. 2011) and they result from the zonal pressure gradient forged by the Atlantic subtropical anticyclone and the western flanks of the Asian monsoon heat low (Bitan and Saaroni 1992; Saaroni and Ziv 2000; Alpert et al. 2004; Saaroni et al. 2010). The cool air advection of the Etesian winds counterbalances the adiabatic warming of the mid- and upper level subsidence, maintaining in this way a thermal balance over the eastern Mediterranean. Moreover, Ziv et al. 2004 have identified a significant correlation between these factors, which likely stems from the Asian Summer Monsoon teleconnection exerting an influence on both the Mediterranean surface and mid- and upper-troposphere dynamics. Rodwell and Hoskins, 1996 demonstrated this linkge, showing that diabatic heating released by the Asian monsoon convection and precipitation triggers a Rossby wave pattern response, which propagates westward, interacts with the mid-level westerlies, and finally induces subsidence and hot and dry conditions over the eastern Mediterranean and the Sahara. This mechanism has been corroborated in several observational and modeling studies (Tyrlis et al. 2013, Rizou et al. 2015, Cherchi et al. 2014, Cherchi et al. 2016). On the other hand, the impact of the monsoon on the Etesian winds has been shown (Rodwell and Hoskins 2001) to be a direct result of changes in the subsidence over EMED, which via Sverdrup's equation trigger changes in the low-level northerly flow (i.e. the Etesians).

This agrees with Ziv et al. 2004 who pointed that changes in the low-level monsoon heat low, which expands westward across Arabian Peninsula, could modulate the zonal pressure gradient and the concomitant Etesians.

The geographic location and socio-economic state of the Mediterranean makes the population in this region particularly vulnerable to climate change. The southern part of the Mediterranean, which is dominated by agricultural activities, is especially sensitive to prolonged water shortages and their consequences, such as drought and wildfires. Giorgi (2006) found this region to be particularly responsive to projected climate change and identified it as a climate hot spot. In fact, both CMIP3 (Giorgi and Lionello 2008, Hanf et al. 2012) and CMIP5 future projections region (Diffenbaugh and Giorgi 2012, Alessandri et al. 2014, Mariotti et al. 2015, Feng et al. 2014) indicate a very strong warming and reductions in precipitation during the summer season. These changes can severely impact water and food security.

At the same time, observational studies have yet to find unambiguous evidence of decreasing precipitation in the recent decades (Blade et al. 2012b, Giorgi and Lionello 2008). Blade et al. (2012) argued that impacts of the summer NAO teleconnection on the European hydroclimate are underrepresented in CMIP3 models, thus questioning the credibility of future summer climate projections for the region. The underrepresentation of the simulated impacts of SNAO could spuriously amplify projected Mediterranean warming and drying. Kelley et al. (2012) indicated that CMIP5 models show a rather modest improvement in the simulated regional hydroclimate, most likely due to increased horizontal resolution. Historical simulations of CMIP5 models still differ from the observations, for example by showing a strong wetting over the northwestern parts of Europe and drying over the southwestern parts of the Mediterranean (e.g. Kelley et al. 2012), though some earlier lower resolution models do show strong drying over many, though not all, parts of north west Europe as well (e.g. Rowell and Jones, 2006). These inconsistencies do not add to the credibility of the current future projections for the Mediterranean and suggest that the severe simulated regional warming and drying requires further investigation, likely using higher resolution models. A further caution is evidenced by the fact that particularly over the last half century the SNAO and the summer European atmospheric circulation as a whole have shown strong multi-decadal variability (Linderholm and Folland, 2017), just as the winter NAO (Scaife et al. 2008). There is also paleoclimate data evidence of related multi-decadal to century timescale variations in the SNAO and Mediterranean climate since 1441 (Linderholm et al, 2009).

The interpretation of the projected future severe warming over the eastern Mediterranean region remains debatable. Cherchi et al. (2016) attempted to interpret the projected summer changes in the region from the perspective of the monsoon –desert mechanism (Hoskins 1996, Rodwell and Hoskins 1996), which links the hot and arid climate of the eastern Mediterranean to the South Asian monsoon rainfall. This mechanism, as shown in the idealized simulations of Rodwell and Hoskins (1996), can be enforced by the diabatic heating of the monsoon convection, which triggers westward propagating Rossby waves and a subsidence and warming localized over the eastern Mediterranean. Given the fact that most CMIP5 models project an increase in the future Asian Monsoon precipitation, one would also expect a strengthening of a subsidence in the eastern Mediterranean. However projected changes indicate rather opposite tendencies of the subsidence in this region, despite a strong severe drying and warming. Cherchi et al. (2016) could not unambiguously resolve this inconsistency, suggesting an explanation associated with either changing representation/impacts of the "desert-monsoon" mechanisms or the emerging presence of non-linear processes in the regional surface circulation.

On the other hand, Seneviratne et al. (2006) identified soil moisture-temperature feedbacks as a dominant

factor controlling summer temperature variability in the Mediterranean and Central Europe in a changing climate. Soil moisture-climate feedbacks were also linked to a non-linear warming of hot extremes in climate change projections for the Mediterranean (Diffenbaugh et al. 2007). Hirschi et al. (2011) confirmed the effect of soil moisture availability for hot extremes in observations in Southeastern Europe and found also that the soil moisture-temperature feedbacks in RCMs are often overestimated over Central Europe. Some studies argued that the deficiencies in the atmosphere - land surfaces feedbacks are a primary cause of a strong summertime warm bias in most of the CMIP3 and CMIP5 models, which spuriously amplifies the projected future temperatures (Christensen and Boberg, 2012, Mueller and Seneviratne, 2014).

Accordingly, in this study, we,: a) analyze future summer climate changes over the Mediterranean region and b) investigate the possibility of emerging new regional climate regimes, describing them, and quantifying their contribution to the projected future changes over Europe. Identifying a regional signal attributed to a particular mechanism or climate regime is not an easy task, given the complexity of the climate in the region. This complexity stems not only from the complex morphology of the region, but also from the teleconnections acting on yearly-to-multi-decadal timescales (e.g. SNAO), and multi-decadal changes caused by anthropogenic gases and aerosols. Addressing these issues requires integrations at high spatial resolution, control runs with greenhouse gas and aerosol compositions being held at the fixed levels and well represented land-atmospheric feedbacks between soil moisture and precipitation. Hence, here we use control, historical and future simulations of the GFDL CM2.5 model (Delworth et al., 2012), that incorporates higher spatial resolution and improved land model (LM3), likely improving the simulated hydroclimate over many continental regions including Europe.

In addition, we create an analysis of the Mediterranean summer climate and interpret the results through the prism of large-scale circulations, teleconnections and the regional factors. Section 2 describes the model and experiments used, the dataset for comparison and the methodology. Section 3 focuses on the summer time-mean climatology of the region, as well as its teleconnections. It evaluates the performance of the model in terms of the simulated regional precipitation, as well as large-scale circulation features, which shape the summer regime of the Mediterranean climate. It also examines the main components of internal variability dominating atmospheric circulation over the Euro-Atlantic region, such as the summer NAO, and their impact on Mediterranean climate. The last part of this section focuses on a representation of key dynamical features shaping the climate regime over the eastern Mediterranean, i.e. including the linkage between the mid- and upper-level subsidence and the low-level pressure gradient (and the associated Etesian winds) together with its coupling with the Indian Monsoon. Section 4 investigates future climate changes over the Mediterranean derived from the model projections. It examines the regional changes from the perspective of large-scale circulation over the Euro-Atlantic and associated summer NAO teleconnections. The derived regional changes are also interpreted in the context of the changing relationships between the dynamical factors governing the eastern Mediterranean. Again, the long control run is used to verify whether the derived changes in the eastern Mediterranean climate regime can be attributed to the local effects of the warming Mediterranean and how these effects will impact the whole Mediterranean and European climate. Section 5 discusses and summarizes the main results.

2. Data and Methods

2.1 Coupled model and experiments

The coupled model use in this study is the Geophysical Fluid Dynamics Laboratory (GFDL) CM2.5. It has an

atmospheric and land surface horizontal grid scale of approximately 50 km with 32 levels in the vertical. The horizontal grid scale of the ocean increases from 28 km in the tropics to 8-11 km in high latitudes. CM2.5 incorporates a new land model (LM3), with an enhanced representation of soil moisture and land-atmospheric feedbacks between soil moisture and precipitation (Milly et al. 2014, Berg et al. 2016). Details of the CM2.5 model features can be found in Delworth et al. (2012). The representation of the summer precipitation climatology in CM2.5 is also compared using a 4000-years control run of GFDL CM2.1, that is the CM2.5's predecessor. CM2.1 incorporates a grid scale of 2° latitude x 2.5° longitude for the atmosphere. The ocean resolution is variable being approximately 1° latitude x 1° longitude, with a finer meridional resolution in the tropics. The CM2.1 atmospheric model has 24 vertical levels (Delworth et al. 2006). The ocean component CM2.1 and CM2.5 consists of 50 levels in the vertical. Future changes projected with CM2.5 are compared with that derived with the CSIRO-Mk3-6-0 model (1.9° x 1.9° horizontal resolution for teh atmosphere), which includes the ocean component based on the GFDL ocean model. This choice was determined by the fact that future projections of CSIRO-Mk3-6-0 model, unlike CM2.1, follow the same protocol of forcing scenario, i.e. the IPCC RCP8.5 scenario (Meinshausen et al. 2011, Riahi et al. 2011), as those of CM2.5.

The set of experiments performed using CM2.5 are listed in Table 1 and it consists of control simulations (hereafter CTRL) and 5-members ensembles of historical simulations (hereafter HIST), and of future projections (hereafter PROJ) performed with CM2.5. The CTRL simulation consists of a 1000-year integration, where greenhouse gas and aerosol compositions are held fixed at the levels of the year 1860. In HIST and PROJ ensembles, the forcing follow the protocols of the Coupled Model Intercomparison Project Phase 5 (http://cmip-pcmdi.llnl.gov/cmip5/forcing.html). For the historical period (1861-2005), the radiative forcings are based on observational estimates of concentrations of well-mixed greenhouse gases (GHG), ozone, volcanoes, aerosols, solar irradiance changes and land-use distribution. While for the future (2006-2100) the radiative forcing follow an estimate of projected changes defined in the IPCC RCP8.5 scenario. This scenario assumes high population growth, slow technological change and energy intensity improvements, and a lack of developed climate change policies, resulting in large energy demand and GHG emissions.

2.2 Datasets used for comparison

The simulated features of large-scale circulation are compared with reanalysis data of monthly pressure at mean sea-level (hereafter SLP), wind vectors at the 850hPa and 200hPa levels, and vertical velocity at 200hPa for the period 1979-2017. Reanalysis data is provided by the NCEP-DOE AMIP-II Reanalysis 2 with 2.5° x 2.5° horizontal resolution and 17 vertical levels (Kanamitsu et al., 2002; https://www.esrl.noaa.gov/psd/data/gridded/data.ncep.reanalysis2.html).

The simulated precipitation is compared with the seasonal time-averaged precipitation provided by the University of Delaware (V4.01), Legates and Willmott 1990; http://climate.geog.udel.edu/~climate/html_pages/README.ghcn_ts2.html (last access: July 2018). This is a global gridded land data set with 0.5° x 0.5° horizontal resolution for the period 1980-2015. For the same period we use also EOBS precipitation data set provided E-OBS dataset from the EU-FP6 project UERRA (http://www.uerra.eu) and the Copernicus Climate Change Service (Cornes et al. 2018, version 17), provided at 0.25° x 0.25° horizontal resolution.

The observational analysis of the summer North Atlantic Oscillation (section 3.2) is carried out using July-August mean sea level pressure (SLP), provided by NOAA/ESRL PSD 20th Century Reanalysis version 2c (Compo et al. 2006, https://www.esrl.noaa.gov/psd/data/20thC_Rean/). The spatial patterns of the dominant component of the SLP variations are computed with Empirical Orthogonal Function (EOF) analysis, over the

domain [25°-70°N, 70°W-50E°], following Folland et al. 2009. The robustness of the pattern is tested against chosen periods of different length.

The relationship between the SNAO and the North Atlantic storm track is derived by computing correlations between the SNAO index and the proxy of storm track in July-August. The storm tracks are represented with the standard deviation of the daily geopotential height at 300 hPa, following Folland et al. 2009. The data is a priori filtered using a Butterworth filter with a bandwidth of 2-8 days. The storm tracks are derived for the 1950-1990 and 1970-2011 periods, using NCEP/NCAR 1 data (Kalnay et al. 1996), provided by the NOAA/OAR/ESRL PSD, Boulder, Colorado, USA, from their Web site at https://www.esrl.noaa.gov/psd/.

2.3 Analysis methods

The representation of the simulated large-scale atmospheric circulation over the Mediterranean is analyzed using CTRL runs' monthly mean fields of the lower, mid- and upper- level dynamics over the region covering southern Europe, North Africa and South Asia [30°N–50°N, 30°W–110°E]. The analysis of the simulated SNAO teleconnection focuses on the Euro-Atlantic region. In the analysis of the eastern Mediterranean climate, we define region of focus as EMED [30°-36°N, 36°-42°E]. We will also refer to the eastern Mediterranean land region, which includes: Syria, Lebanon, Israel, Jordan, as the Levant region.

The time-mean large-scale circulation features are analyzed based on the monthly means of hydro-meteorological variables for the summer (June, July and August, hereafter JJA) season. Future changes are estimated by comparing the climatology at the end of the twenty-first century (i.e. 2061–2099, hereinafter future) of the RCP8.5 scenario with that at the end of the twentieth century (i.e. 1961– 1999, hereinafter present) of the historical simulation using monthly mean fields for the summer season.

The teleconnection of the Mediterranean climate with SNAO is analyzed using the full (1000 year) CTRL run (section 3.2), as well as the historical and future runs. The SNAO is defined as a lead component of SLP vector time series over the Euro-Atlantic region [25°N–75°N, 70°W–50°E] in "core summer" (July-August), following Folland et al. 2009. The choice of the time window is determined by the fact that the temporal behavior of the SNAO in significantly correlated only within these two months. The impact of this teleconnection on Mediterranean climate is estimated using correlations between SNAO PC time series and the regional temperature and precipitation, using the long CTRL experiments and the historical and future ensembles. The evolution of the SNAO fingerprint in the 20th and 21st century is analyzed by projecting the vector time series of HIST and PROJ experiments (240 yrs, 1861-2100) on the SNAO eigenvector derived from the CTRL run. To analyze potential changes in the spatial pattern of SNAO and associated impacts, the EOF analysis is applied independently to each of the HIST and PROJ ensembles, in the period 1950-2010 and 2040-2100, respectively, detrending the timeseries before computing the EOF. In both epochs, the analysis has been also tested for shorter periods (i.e. 50 and 30 years), which did not change the results in qualitative terms. Each of the five SNAO time series for the 1950-2010 and 2040-2100 periods were correlated with the respective detrended precipitation fields.

The summer climate regime of the eastern Mediterranean (hereafter EMED) is examined from the perspective of the regional mid- and upper-tropospheric subsidence and its physical linkage with the surface circulation (section 3.3). The seasonal variability of the subsidence over the eastern Mediterranean is derived from EOF analysis applied to vertical velocity (omega) fields at 500 hPa, and also at 300 hPa over the region

covering the Mediterranean, North Africa and Middle East in July season. The physical linkage between the subsidence and surface circulation is estimated using correlations between the time series of the first EOF component (PC1) and the regional sea level pressure, geopotential height and wind vectors at 850 hPa. The relationship between the EMED region dynamics and the Indian Summer Monsoon is estimated by computing additional correlations with precipitation, outgoing long wave radiation, and the vertically integrated water column. The analysis shows the correlations computed using time series of EOF omega at 500 hPa, but the correlations using EOF omega 300 hPa were almost the same. The results of the analysis are shown for July, when the magnitude of subsidence and the Etesians is at its maximum and the response of the Rossby waves to monsoon rainfall is also strongest (Tyrlis et al. 2012, Lin et al. 2007, Lin et al. 2009). The results derived for June and August are shown in the Supplementary Information.

Future changes in the dynamical linkages governing the summer climate regime over the eastern Mediterranean were analyzed by comparing the five-decade long samples for July, i.e. 1960-2010 and 2050-2100. The linkage was calculated in a similar manner to that of the control run using correlations between the time series of the EOF over the EMED region subsidence and the atmospheric surface circulation fields. All EOF time series were computed by projecting the respective run on the eigenvector derived from the control run. The correlations were derived for each run (historical and future, respectively), using a priori detrended timeseries. The final result shows the ensemble mean for the five-member historical and future correlations.

An additional analysis investigates the potential influence of the local temperature (i.e. in the EMED region) on the derived local dynamical relationships (section 4.3 and Supplemenary Material). Therefore, the derived correlations were differentiated between samples with the 300 warmest and the 300 coldest summers (July) over the Mediterranean, chosen from the control run time series. Their selection is based on surface temperature in the EMED region. Additionally, a diagnosis of temperature impacts on the regional atmospheric circulation was performed using composite differences between the two temperature samples and the associated relative humidity, sea level pressure, wind components, geopotential height, vertical velocity and precipitation. The results were corroborated by testing their sensitivity to the precise choice of the region.

3 Summer mean present climate and teleconnections over the Mediterranean region

3.1 Simulated summer mean Mediterranean climate

Figure 1 demonstrates that the model captures the subtropical low-tropospheric circulation with high fidelity when compared with the reanalysis (NCEP-DOE). It reproduces accurately the zonal pressure gradient over the Mediterranean, both in terms of pattern and magnitude, forged by the difference between the subtropical anticyclone over the North Atlantic and the massive Asian monsoon heat low. The latter extends westward, through the Arabian Peninsula towards the Levant region and southern Asia Minor. Concomitant to the zonal pressure gradient and adjustments to the regional orography is a persistent west-northerly flow over the central and eastern Mediterranean (i.e. the Etesian winds). The model reliably captures its local-scale features, created by adjustments to the regional topography. This includes a local wind maximum centered over the Aegean Sea and its southern extension reaching the Sahel region. These northerlies are also channeled through the Red Sea Straits and the Persian Gulf, reaching the Indian Ocean.

Figure 2 shows that the model reproduces the location and magnitude of the summer subtropical mid-troposphere anticyclone, which spreads from the eastern Mediterranean across the South Asia. The simulated mid-troposphere also captures the location and a realistic magnitude of the persistent mid-troposphere (500

hPa) subsidence (positive omega) which creates the exceptionally hot and arid climate of the eastern Mediterranean. This subsidence gradually decreases towards the Iranian Plateau, which together with ascending motion over the South Asian monsoon region, creates a large-scale time-mean zonal gradient. The simulated zonal gradient is well shown (Fig 3a) by a vertical cross-section of vertical velocity (omega) averaged over 20°-34°N between the east Mediterranean region (positive omega means strong subsidence) and the South Asia (negative omega means ascending air). This characteristic gradient agrees well with its observational counterpart (Fig 3b) both in terms of magnitude and pattern. Importantly, the model captures the observed local maximum of the eastern Mediterranean subsidence located at middle-tropospheric levels (300-700 hPa), the region most sensitive to the impact of the Indian monsoon.

Figure 4 shows climatologies of the Mediterranean precipitation provided by the observations, the CM2.5 control run, and also its low-resolution (CMIP3) predecessor, i.e. CM2.1 at their original horizontal resolutions. Although both CM2.1 and CM2.5 depict the general spatial features of the climatology (i.e. large values in the northern Mediterranean, particularly over the Alps and the Balkans), the former introduces large biases (up to 50%) in regions with sharp spatial gradients. CM2.5 resolves much better the spatial features of precipitation, clearly indicating the advantages of higher horizontal model resolution for regions with complex orography. However, precipitation magnitude in most mountainous areas, e.g. the northern Iberian Peninsula, the Alps and over Asia Minor, is larger than in both observational data sets, i.e. U. Delaware.and EOBS. The climatology in CM2.5, in terms of pattern and magnitude, seem to be much more consistent with the EOBS data set. However, due to a relatively large observational uncertainty in many mountainous areas, it is difficult to validate the model rainfall climatology in these regions. Kelley et al. (2012) suggested a modest improvement in CMIP5 models compared to CMIP3 in representing precipitation over the Mediterranean region, most likely associated with increased horizontal resolution. However, none of the CMIP precipitation climatologies could realistically capture the complexity of regional features (e.g. local maxima over the northern Asia Minor and the Balkan coast) to such a high degree as in CM2.5. Overall, our analysis indicates that the high-resolution CM2.5 control run provides a realistic mean representation of the surface- and upper-tropospheric circulation over the Mediterranean. The model skillfully simulates sharp gradients of precipitation over the morphologically complex terrain and its climatology is considerably better than its low-resolution predecessor, the CM2.1 model.

3.2 The impact of the summer North Atlantic teleconnections on the Mediterranean region

The origin of the multi-decadal signal of SNAO has been linked (Knight et al. 2006, Folland et al 2009, Linderholm and Folland 2017) to the Atlantic Multidecadal Oscillation, which originates from internal variations in thermohaline circulation (Knight et al. 2005, 2006, Delworth and Mann 2000; Enfield et al. 2001), but for the recent decades also from anthropogenic sources (Rotstayn and Lohman 2002; Mann and Emanuel 2006). The imperative of the following section is to test the capability of the model to simulate the SNAO as an independent, internally generated climate component, which would prove the physical validity of the statistically-derived component. The SNAO is defined as a leading eigenvector of the atmospheric circulation over the North Atlantic region [25°-70°N, 70°W-50N°]. For this purpose we use the monthly SLP output (July-August) of the full period (1000 years) of the CTRL experiment (Table 1). The analysis is also repeated for the HIST and PROJ runs. The results are compared with the observational analysis, using SLP provided by the 20CR dataset in the period 1870-2010. However, allowing for the fact that a) circulation over the SNAO region is influenced by different key factors at different times, giving rise to time-varying dominant modes of apparent internal variability; and b) each simulation represents a different, non-

deterministic state of internal climate variations, one should not expect to obtain from each run a replica of the observed SNAO component.

3.2.1 Spatial pattern of SNAO

Considering the first two EOFs in the CTRL SLP averaged in summer, EOF1, representing the SNAO, clearly dominate the summer SLP variations, explaining twice as much total variance as EOF2. Moreover, the percentages of explained variance (34% and 15%) resemble those of the observations-based EOF1 and EOF2 in Folland et al. 2009, i.e. ~28% and ~14% respectively. In the following we focus on the leading pattern (hereafter called CTRL EOF1).

Figure 5a depicts spatial pattern of CTRL EOF1. The derived dipole resembles the observed SNAO signature (e.g. Folland et al. 2009), including a distinct northward shift when compared to the winter counterpart (shown e.g. in Barcikowska et al. 2017). The dipole pattern has a northern lobe over the south-western flank of Greenland and a southern lobe centered north of the Azores in the vicinity of ~45°N, 30°E. At its positive phase SNAO is manifest with negative anomalies in the former and positive anomalies in the latter region, thereby strengthening the meridional SLP gradient over the North Atlantic. The pattern is similar also when analyzed for the single months July and August (not shown). The simulated SNAO pattern is almost identical to the one derived from the HadCM3 model control run, as shown in Folland et al. 2009.

Further analysis indicates also that the signature of the simulated SNAO is much more consistent with the observed one before 1950s, rather than in the recent six decades. Figure 6 depicts patterns of EOF1's derived from four 50-yr periods of the 20CR reanalysis (i.e. a. 1870-1920, b. 1900-1950, c. 1940-1990, d. 1960-2010), indicating clearly their evolution in time. Similar results were obtained for the independent 40-yr periods (1851-1890, 1891-1930, 1931-1970, 1971-2010 in Figure SI1). The EOF derived for periods before 1950s (shown here for 1870-1920 and 1900-1950) closely resembles the SNAO simulated in the model (Fig 5a), i.e. including the northern centers of action at southern Greenland and with the southern lobe situated north of the Azores (~45°N, 35°E). In contrast, the EOF derived for 1960-2010 or 1971-2010 exhibits a weak northern lobe and a much stronger southern lobe, with the latter being also shifted north-east, towards the British Isles. These differences are consistent with other observational analysis of the recent six decades (i.e. Blade et al. 2012 and Syed et al. 2012).

Analysis of the HIST runs shows that the pattern of the leading EOF also evolves in a similar way to the observations-based SNAO pattern (Figure 6). For the early observational period (1870-1920), all the derived SNAO signatures, i.e. EOF derived from all HIST runs (Figure 6b, Figure SI2 left column), observations, and CTRL (Figure 5a) resemble the SLP dipole with the northern lobe over Greenland and the southern lobe located north of the Azores around 40-45ºN. In contrast, for the most recent period (1960-2010, Figure 6g, h) both observations and HIST runs depict SNAO with the weaker northern lobe and southern lobe being shifted north-eastward, towards the British Isles. These changes are found in 4 out of the 5 HIST members available, when comparing the periods 1870-1920 and 1960-2010 (Figure SI2). This tendency slightly intensifies when the more recent period is extended towards the future using PROJ members (e.g. 1970-2030, 1970-2060 Figure SI3). Considering the nature of HIST experiments, this analysis suggests that the anthropogenic forcing, which is the only deterministic factor for them, is likely an important contributor in shaping the SNAO, and hence explaining to some degree the temporal evolution of its spatial signature in the 20th century.

3.2.2 Impact of SNAO on the Mediterranean hydroclimate

Figure 5 indicates that the simulated SNAO yields a large-scale fingerprint in the precipitation, geopotential height and temperature over the North Atlantic and Europe, which largely resembles the observed one (e.g. Folland et al. 2009, Blade et a. 2012). This includes a distinct tripolar pattern of precipitation anomalies with the lobe over the southern Greenland, over northern Europe and its vicinity over the North Atlantic, and over southern Europe and most of the Mediterranean region (Fig 5c). The derived SNAO teleconnection at its positive (negative) phase, manifested in the positive (negative) SLP anomalies over its southern lobe (Fig 5a), is linked with an anomalous drying (wetting) over northwestern Europe, but with anomalous wetting (drying) over the Mediterranean (Fig 5c).

The simulated location of the southern SLP node is located southwest of the British Isles, and so its largest impact is in this region with negative correlations reaching a value of about -0.7 (Fig 5a). The maximum impact of the observed teleconnection, as shown in Folland et al. 2009, is of similar magnitude and exceeds ~0.6, though its location is centered over the British Isles. This difference directly relates to the difference in the center of the observed southern node of SNAO, when compared from that in CRTL runs, discussed in the previous section. For Mediterranean hydroclimate, the consequences of a positive SNAO phase are the inverse of those in northwest Europe and also of smaller magnitudes (i.e. ~0.2-0.35). Corresponding wet anomalies are centered over Italy, the central and southeastern Iberian Peninsula, and Asia Minor.

The pattern and magnitude of SNAO teleconnection presented here is largely consistent with the one derived from the GFDL CM2.1 model, the low-resolution predecessor of CM2.5 (Blade et al. 2012). The CM2.5 correlation coefficients over the Mediterranean are also quite similar to those of the observations-based SNAO in Folland et al. 2009, exceeding locally 0.3 (1900-1998). In contrast, Blade et al. 2012, using a shorter data set (EOBS, 1950-2010), found much larger correlations, locally exceeding 0.6. This disparity may likely stem from the difference in the length of the analyzed data sets and differences in contributing factors. For example, the SNAO time series, as defined by Blade et al. 2012, are largely shaped by a multi-decadal signal of both the natural and anthropogenic origin. By contrast, anthropogenic climate components are not included in the CM2.5 control run and the simulated SNAO teleconnection stems predominantly from the internal climate variations on interannual time scales.

The impact of the SNAO on the northern Europe and southern Europe hydroclimate has been explained through different mechanisms. The teleconnection between SNAO and the northwestern Europe hydroclimate has been straightforwardly explained with impact of the North Atlantic storm tracks, which are controlled by the large-scale circulation in this region. Folland et al. 2009 have shown, using NCEP data, that a positive (negative) SNAO index relates to the North Atlantic storm tracks being shifted northward (southward) towards the northwestern (southwestern) Europe. Our analysis, using the SNAO index derived from 20CR, and the storm tracks proxy derived from NCEP, confirms this relationship (Figure SI4). More importantly, the strength of the derived relationship depends on the chosen period. For example, the derived correlations are distinctively stronger in the earlier period, i.e. 1950-1990, when SNAO resembles a dipole pattern (Figure 6e), than for the latter period (1970-2011), when the SNAO better resembles a monopole-type pattern located over the British Isles (Figure 6g). These results are consistent with the notion that the monopole-like version of the SNAO, derived from the most recent decades of observations, is contaminated by other climate components. Hence it is not necessarily the most plausible representation of the SNAO. However, addressing this issue as well as verifying the simulated linkage between the SNAO and the North Atlantic storm tracks are beyond the scope of this study and it could be eventually subject for future research.

The impact of the SNAO on the Mediterranean hydroclimate (shown by in observations by Linderholm et al. 2009) can be better explained through associated changes in a mid- and upper-tropospheric geopotential height, consistent with Blade et al 2012. Correlations derived between the SNAO time series and 500hPa geopotential height (Fig 5b), show the strongest influence over the western and central Mediterranean, i.e. the Iberian Peninsula, Italy and to a smaller extent the Balkan coast. Well collocated with this pattern are correlations with precipitation and surface temperature, although for the latter the impact of the SNAO seems much smaller. Hence, anomalous precipitation in these regions during the positive SNAO phase likely stem from an anomalous mid- and upper tropospheric trough, associated cooling, and intensified potential instability over the central Mediterranean.

Overall, the results presented in this section demonstrate that CM2.5 is capable of simulating SNAO teleconnections and their contribution to Mediterranean hydroclimate. The associated physical mechanisms are consistent with observational findings and other modeling studies employing older generations of models.

On the other hand, the impact of SNAO on surface temperature in the Mediterranean shows discernible differences, compared to the observational studies (Blade et al. 2012, Folland et al. 2009). For example, the maximum of the derived correlations in CM2.5 is located over the Iberian Peninsula (exceeding locally ~0.35). In contrast, both studies show the maximum of the correlations shifted towards central and eastern Mediterranean, although with a significant disparity in the derived magnitudes. While the former study suggests the maximum magnitude of correlations reaching 0.7-0.8, the latter study suggests correlations twice as smaller when using a longer data set and low-frequency component removed. Hence the impact of SNAO on the European temperatures remains a debatable issue and requires further investigation in the future.

3.3 Summer climate regime over the eastern Mediterranean

In this section we investigate the ability of the CM2.5 control experiment to reproduce the summer climate regime over the eastern Mediterranean (EMED, as defined ins Sect. 2), including the relationship between the surface dynamics and the mid- and upper-tropospheric circulation over the region and its teleconnection with the Indian Summer Monsoon (hereafter ISM). Here we show results for July alone but those for June and August are shown as Supplementary Information. This choice is driven by the fact that the magnitude of subsidence and the Etesians is at its maximum in July while the response of the Rossby waves to monsoon rainfall is also strongest (Tyrlis et al. 2012, Lin et al. 2007, Lin et al. 2009).

Figure 7d, (see also Ziv et al. 2004, Tyrlis 2012) shows that the model captures skillfully the observed features of the regional relationship between the mid- and upper-tropospheric subsidence and surface circulation. The relationship is depicted in Figure 7 as correlations computed between time series of EOF1 (Figure 7a) of the mid and upper- tropospheric vertical velocity (omega) over the Mediterranean and those of geopotential height at 850hPa, wind vector, outgoing longwave radiation and precipitation. EOF1 derived either for omega at 500 hPa or 300 hPa, explains the dominant amount of variance (~33% and 35%, respectively). Its spatial pattern closely resembles the simulated and the observed (Tyrlis et al 2012, Ziv et al. 2004) key feature of the mid- and upper omega summer climatology, i.e. with a maximum located near Crete. The correlations (Figure 7b,c), derived between the EOF1 500hPa and the regional surface circulation, depict a physically consistent linkage (Figure 9d, Ziv et al. 2004, Tyrlis 2012) between strengthening of the subsidence over the EMED and strengthening of the zonal pressure gradient over the Mediterranean and thus the Etesians over the EMED.

The Etesians spread southward from the Aegean Sea, through Egypt and towards the Sahel which is consistent with observational findings underlining the role of the Etesians in regulating the moisture transport over Africa and hence for regulating the African monsoon (Raicich et al. 2003, Ziv et al 2004, Lelieveld et al. 2002; Rowell 2003). The northerlies intensify also over the Arabian Peninsula as north westerlies, with wind anomalies spreading towards the Gulf of Persia and the Indian Ocean. The simulated pattern agrees well with its observational counterpart, derived by correlating the regional anomalies of omega 500hPa and meridional wind using the detrended NCEP–DOE data set. Note that due to a relatively short data set (1979-2015), the correlations are not significant at the 10% level for some regions and thus not shown, even if they agree well with those simulated, for example the positive correlations in northwest Africa.

This relationship between mid-level subsidence and the low-level circulation is manifested to some extent in the regional summer precipitation and outgoing longwave radiation. Figure 8 shows that correlations derived between the same EOF of omega at 500hPa and precipitation are negative and centered over southern Italy and the Balkans. This implies that the stronger subsidence over EMED may contribute to precipitation reductions in these regions, consistent with the intensified zonal pressure gradient and the associated intensification of the anticyclonic circulation over the western and central parts of the Mediterranean. However, the summer precipitation in the Mediterranean is in general very low and correlations do not exceed 0.3, implying a rather small effect. On the other hand, the EMED subsidence variations show much stronger correlations (up to 0.8) with the outgoing long-wave radiation (OLR) over the region (Figure 8). This is consistent with the impact of the adiabatic descent and associated radiative cooling in dry regions under clear sky conditions.

The simulated relationship between the interannual timescale variations in EMED region and the northwestern parts of India (Fig 8) is consistent with the features of the observed teleconnection with the Indian summer Monsoon (ISM) (Hoskins et al. 1996, Hoskins et al. 2001, Tyrlis et al. 2012, Ziv 2004, Cherchi et al. 2014). The variations of the EOF of omega at 500hPa show significant and relatively high correlations with the three monsoon indices, i.e. subsidence over EMED is negatively correlated with OLR (up to -0.45), and positively correlated with vertically integrated water vapor (up to 0.6, not shown) and precipitation over the northwestern parts of India (up to 0.3). This implies a connection between anomalously stronger subsidence over the EMED region and the intensified Indian summer monsoon. Consistent with this linkage are intensified southerly winds over the Arabian Sea, which feed the ISM with moisture (Figure 6b, c), and a deeper heat low spreading west from India towards the Arabian Peninsula and the Sahel. The latter intensifies the zonal pressure gradient over the Mediterranean, which illustrates how the ISM impacts the low-level circulation in Mediterranean as suggested in Ziv et al. 2004.

These results suggest that CM2.5 is capable of capturing the most prominent features of the summer climate regime over the EMED: the mid- and upper tropospheric subsidence over the EMED and the low-level Etesian winds. Moreover, these results also show that the model reproduces their links with the ISM. Changes in these interactions over the EMED and their teleconnections may give rise to pronounced effects on local Mediterranean summer temperature regime. Accordingly, the next section investigates the projected future Mediterranean climate, interpreting this through changes in large-scale circulation as well as through local relationships and teleconnections.

4. Climate changes in the 21st century

4.1 Comparison of future and present summer climate

In CM2.5, the projected changes in large-scale circulation features over the Euro-Atlantic region and west Asia correspond to a large extent to those seen in the CMIP3 and CMIP5 projections. Figure 9 depicts changes in the summer surface atmospheric circulation, as shown by SLP in JJA and wind vectors computed at the original model horizontal resolution (~0.5°). The most prominent feature over the Euro-Atlantic region, a northward shift and strengthening of the meridional SLP gradient, and hence the meridional circulation cells, is a typical fingerprint of anthropogenic climate change (Collins et al. 2013). The associated anomalous bipolar SLP pattern shows negative (cyclonic) SLP anomalies centered over Greenland and positive (anticyclonic) SLP anomalies centered southwest of the British Isles. This pattern closely resembles the fingerprint of the CTRL-based SNAO. The projected positive SLP anomaly is however shifted slightly north east of the CRTL SNAO, so it is likely that the anthropogenic fingerprint will project on the positive SNAO phase, quite like as found by Folland et al. 2009 for HadCM3 and HadGEM1.

CM2.5 projections also indicate negative SLP anomalies over North Africa, the eastern Mediterranean and the Arabian Peninsula, which are accompanied by a very strong warming exceeding 6°C. These changes, together with an anomalous convergent flow and pronounced anomalies of ascending air at low-and mid-tropospheric levels (Figure 3c, Figure SI5) over the Arabian Peninsula, contribute to the intensification of the Persian trough. Although the Persian trough constitutes an extension of the southwest Asian Monsoon heat low, the future SLP over the monsoon region shows positive anomalies. This indicates a weakening of the monsoon heat low and, correspondingly, of the northerly flow over the Persian Gulf. It is also worth noting that the anomalies of ascending motion over the Levant region and the Arabian Peninsula, together with an anomalous subsidence over the center, north-eastern Mediterranean, and Asia Minor, create a distinct gradient in the vertical velocity changes. This gradient is particularly evident in July (Figure SI5), due to a magnified intensification of the heat low and anomalous ascending motion over the Levant region.

The projections also show clear differences, both quantitatively and qualitatively, when compared with the CMIP5 multi-model ensemble of RCP8.5 projections (Collins et al. 2013) and the CMIP3 ensemble of the A1B scenario (Giorgi and Lionello 2008). The intensity of the changes over the Euro-Atlantic region shown by CM2.5 is much larger (Figure 9) than in the CMIP5 ensemble average (Collins et al. 2013, Fig 12.18), even when the analysis is conducted at the CMIP resolution. For example, one of the most robust features of the anthropogenic fingerprint, i.e. anomalous positive SLP anomaly in the vicinity of British Isles, is almost twice as intense (~up to 3hPa), when analyzed at 2° horizontal resolution. Moreover, in contrast to the CMIP5 ensemble, the projected CM2.5 positive SLP anomalies over the British Isles expands through northwestern Europe to the southeastern regions: this intensifies the anticyclonic circulation over the western and central Mediterranean. The CMIP3 ensemble (Giorgi and Lionello et al. 2008) show similar tendencies but with a much smaller magnitude confined just to northwestern Europe. On the other hand, the CMIP5 ensemble shows negative SLP anomalies spread over the whole Europe, North Africa and Arabian Peninsula. These differences between the CM2.5 and the CMIP ensembles yield opposite effects on the Mediterranean surface circulation. In CM2.5, positive SLP tendencies to the west of the Mediterranean and the strengthening of the heat low in the eastern Mediterranean, Arabian Peninsula and North Africa foster the strengthening of the climatological zonal pressure gradient, and the associated northerly winds over the Aegean Sea. In contrast, the strengthening of the heat low, which expands over the whole Mediterranean, gives rise to a weakening effect on the regional zonal pressure gradient and the northerly flow in the central and eastern Mediterranean (Collins et al. 2013, Fig 12.18).

Analysis of future changes in mean surface temperature and precipitation indicates (Fig 9b,c) a less radical warming and a weaker and less spatially extensive drying over central and southern Europe, when compared to the CMIP3 (Dubrowski et al. 2014), CMIP5 (Collins et al. 2013) ensembles and a high resolution EURO-CORDEX GCM-RCM RCP8.5 multi-model ensemble (Fussel et al. 2017, Jacob et al. 2014, Figure SI6). For regions like the Iberian Peninsula and Asia Minor warming is on average ~2°C lower. The largest difference (more than 3°C) occurs over the southeastern Europe and northern parts of the Balkans, which feature a local minimum of warming ~1°C and wetting tendencies. The latter has not been captured in the CMIP models. For example, the 10-member RCP8.5 ensemble of the CSIRO-Mk3-6-0 model projects (Figure SI6) a strong warming, which over southern Europe exceeds locally ~7°C (e.g. the southern France and Iberian Peninsula), while in the southeastern Europe and northern Balkans it exceeds ~6°C. The multi-model ensemble average of combined GCM–RCM simulations from the EURO-CORDEX initiative (Fussel et al. 2017, Map 3.4, pp. 76) indicates a comparable magnitude of warming, although with local maximum of warming (exceeding 6°C) shifted towards the Iberian Peninsula, while warming over the southeastern Europe and northern Balkans varying between 3.5 and 5.5°C. In both CMIP ensembles the projected very intense warming and drying over the whole European region has been often questioned and linked with a warm summertime bias, caused likely by the deficient representations of moisture-temperature feedbacks. However, some CMIP3 and CMIP5 models, which incorporate a relatively high resolutions (CNRM-CM5 and EC-Earth-DMI, ~1-1.5°, Christensen and Boberg, 2012), although much lower than the CM2.5, feature both relatively low temperature bias and also relatively milder anthropogenic changes.

Furthermore, the gradient of warming between the southwestern and northeastern parts of Europe in CM2.5 is much sharper and shifted southward when compared with these ensembles (see Fussel et al. 2017, Map3.4; Figure SI6). For example, the minimum of warming (1.5-2°C) in the EURO-CORDEX ensemble is located over the southeastern Baltic countries, while in the CM2.5 the minimum expands across the central Europe and southeastward, towards the northern coast of the Black Sea. Hence the latter contributes in CM2.5 to a stark contrast in the warming between the Mediterranean coast including coastal region of Balkans (4-6°), and the inland Balkans together with southeastern Europe (1°C). This temperature gradient (Fig 9b) marks also a clear transition zone between the drying of southwestern Europe and the wetting of northeastern Europe (Fig 9c). This transition zone, analogously to the warming gradient, is much sharper and shifted southward in the CM2.5 projections when compared with the CMIP3 and CMIP5 models (Fussel et al. 2017, Map 3.8). For example, future changes derived from the CSIRO-Mk3-6-0 model ensemble (Figure SI6) feature drying over whole Europe, except Scandinavia. However, the location of the precipitation transition zone among CMIP5 models features large inter-model spread, which makes the magnitude and sign of the changes over large parts of central Europe uncertain (Fussel et al. 2017, Map 3.2).

Owing to its relatively high resolution, CM2.5 also provides more spatially refined information, which includes for example sharper gradients along the coasts or in the mountainous regions. All coastal regions experience reductions in precipitation, expected from the strengthening temperature contrast between the fast warming land and slower warming sea. These reductions are especially pronounced along the northwestern coasts of the Iberian Peninsula, where rainfall is typically larger due to incoming North Atlantic storms. The advantages of the increased horizontal resolution also become apparent for the Levant and the Arabian Peninsula. This is because the low-resolution CMIP models have difficulties with realistically resolving the projected zonal gradient between oppositely signed rainfall tendencies (i.e. drying over the eastern Mediterranean and wetting on the western flanks of the monsoon). This results in a much smaller changes and statistical insignificance.

Finally, the projected magnitude of the strong warming and drying in the Mediterranean shown by CMIP3 and CMIP5 has often been questioned, due to the deficiencies in representing land-atmosphere feedbacks and a weak sensitivity to atmospheric teleconnections such as the SNAO. For example, Blade et al. 2012 argued that the drying projected in most CMIP3 and CMIP5 models is overestimated due to a deficiency in capturing the SNAO teleconnection and its cooling and wetting effects over the Mediterranean associated with a future more positive SNAO. However, our analysis has shown that the regional impacts of the SNAO in CM2.5 (section 3) are almost the same as those indicated by the low-resolution CM2.1 model. This suggests that the difference in the projected future changes between the CM2.5 and previous generation models may stem rather from the other factors such as representation of soil moisture and land-atmospheric feedbacks between soil moisture and precipitation in the LM3 model used in CM2.5 (Berg et al. 2016; Milly et al. 2014).

4.2 Future changes in SNAO- Mediterranean teleconnections

Temporal evolution of the SNAO depicted (Figure 10c) by the ensemble average of the HIST+PROJ runs reveals relatively weak positive SNAO tendencies in the latter half of the 20th century and a much stronger positive trend during the 21st century. However, for the former period each realization features strong internal variations. This is consistent with recent observations of SNAO featuring a rich interannual to multi-decadal variability and a weak positive trend described in section 3.2.1. For the latter period (particularly 2040-2100) the trend becomes strong enough to be discernible in every realization.

Further analysis suggests also subtle changes in the future spatial pattern of the SNAO. Comparison of SNAO signatures in the 1960-2010 and 2050-2100 periods indicates a northeastward movement of the SLP dipole. This feature is also consistent with the projected changes in large-scale circulation over the North Atlantic (Figure 9a) featuring an intensification and northeastward shift of the meridional SLP gradient. Figure 10a,b, shows that the derived northeastward intensification of the SNAO is manifest in the future European hydroclimate. The correlations, derived between the time series of the SNAO principal component and precipitation anomalies, indicate a shift of the southern SNAO lobe towards the British Isles. This corresponds with a stronger influence of the SNAO on the Euro-Atlantic precipitation, i.e. enhanced drying during the positive SNAO phase. The opposite-sign correlations over southern Europe show also a slight increase, particularly for the Iberian Peninsula, southern Balkans and Asia Minor, indicating an increase in the wetting impact of the SNAO on the Mediterranean.

It is important to mention that the intensified future impact of the SNAO over the Mediterranean, i.e. wetting, is not reflected in the overall mean hydrological changes in this region (Figure 9b,c), with the latter indicating rather a strong warming and drying. Hence the key implication of these results is that without the SNAO the future climate drying in the Mediterranean would be even more severe. The inferred contribution of the SNAO that offsets the regional drying is depicted in the following analysis. Figure 10d,e compares the overall regional future changes, derived between 1961-1999 and 2061-2099, with the changes excluding the impact of the SNAO. The comparison shows that without the SNAO contribution the average drying over the southeast and central Iberian Peninsula would intensify from ~-0.4 to -0.65 mm/day, and for the Balkan coast from ~-0.3 to -0.55mm/day, and for parts of Asia Minor from ~-0.6 to -0.8 mm/day. The location of the largest differences is consistent with the location of the intensified impact of the SNAO (Figure 10a,b). It is worth to highlighting that for regions like the Iberian Peninsula, the estimated contribution of the SNAO (wetting) is

comparable with the magnitude of the projected overall drying. This confirms an important role of SNAO and its future changes by offsetting the future drying in the southern Europe.

These results are also consistent with Blade et al. 2012, who emphasized the role of the SNAO in shaping the future Mediterranean climate. On the other hand, our results do not support the theory proposed by Blade et al. 2012, that the regional impact of the SNAO simulated in the CMIP5 models is too weak, thereby causing an excessive warming and drying in the future projections for the Mediterranean. The estimated impact of the SNAO (in terms of pattern and magnitude) in CM2.5 is almost the same as that shown for the CM2.1 (Blade et al. 2012) and yet the CM2.5 projections indicate a substantially less intense warming and drying over southern Europe, compared to CM2.1 (Blade et al. 2012), CMIP3 and CMIP5 ensembles (Collins et al. 2013). For regions like northern Balkans and central Europe CM2.5 indicates even wetting tendencies, in contrast to drying in the CM2.1 runs and CMIP3/CMIP5 ensembles. For these regions CM2.5 even indicates also strikingly weaker warming, compared to the CMIP5 ensemble (Collins et al. 2013; compare for example ~1 to 2°C warming in CM2.5 with ~6-7°C warming in CSIRO-Mk3-6-0 over southeastern Europe). Additionally, the fact that both GFDL models (i.e. CM2.1 and CM2.5) show very small or no SNAO impact in these regions, suggests the influence of other factors than the SNAO are responsible for these discrepancies.

4.3 Future changes in other aspects of the summer climate in the EMED region

This section investigates other projected CM2.5 climate changes in the EMED region, including low-tropospheric circulation and mid- and upper tropospheric subsidence, the main factors that maintain the regional temperature balance. The projected future intensification of the Etesians as well as the weakening subsidence should yield a cooling and wetting effect on that region. Nevertheless, future projections indicate a very strong warming and drying in this region (e.g. Figure 9; Cherchi et al 2016, Collins et al. 2013). This suggests a decreasing influence of the atmospheric dynamics on the temperature balance of this region and an increasing impact of surface warming on surface circulation. The latter is manifested in the intensification of the heat low over Sahara, EMED and Arabian Peninsula, accompanied by anomalous surface convergence and ascending air centered over the maximum warming—the Levant and the Arabian Peninsula.

In the following, we investigate future changes in these factors governing the summer EMED regime by analyzing the stationarity of the local linkages and teleconnections by comparing their representation in the HIST and PROJ experiments. We also compare coupling of the EMED regime with the Indian summer Monsoon and explore the impact of the local surface warming on the regional surface circulation.

4.3.1 Changes in the local and remote relationships with the EMED climate regime

Figure 11 compares the HIST and PROJ five-member ensemble mean correlations, showing substantial qualitative and quantitative differences between the historical and the future periods. The linkage between the EMED subsidence and surface circulation, in terms of pressure, northerly winds over the Aegean Sea (Etesians), as well as their extension towards North Africa and Persian Gulf, is much weaker for 2050-2100. For example, correlations between the EMED subsidence and the northerlies decrease locally (e.g. Persian Gulf) by more than a factor of two (from ~0.7 to ~0.3) between 1960-2010 and 2050-2100. This is consistent with radically decreased correlations with water vapor and precipitation (from ~0.4-0.5 to ~0) over the African monsoon region, which is largely fed by moisture transported by the Etesians.

At the same time, correlations between the EMED subsidence and ISM indices (July), i.e. precipitation and column integrated water vapor (Fig 11e, f), does not change much. In both cases correlations reach 0.5 for precipitation, and 0.6 for the water vapor. For the latter, the maximum correlations only decrease from 0.7 to 0.6. Both patterns are slightly shifted toward the southern parts of India in the future period, consistent with a southward shift of the southerlies over the Arabian Sea that act as a moisture supply for the ISM monsoon.

These results imply generally insignificant changes in the future mid- or upper-tropospheric teleconnection between the EMED and ISM regions. However they do suggest a pronounced weakening of the local linkage between the mid- and upper-tropospheric subsidence and surface circulation over the EMED. Moreover, given that the local linkage serves as a "medium path" for the teleconnection between the ISM and surface circulation over EMED, future weakening of the local linkage will most likely diminish the impact of this teleconnection on the EMED surface circulation. On the other hand, the projected intensification of the heat low over North Africa, EMED and Middle East suggests a growing contribution of surface temperature to the summer climate regime in those regions. Thus in the following section we explore apparent nonlinearities in the summer climate regime of the eastern Mediterranean associated with the local surface temperature.

4.3.2 Nonlinear dependency of the local interrelations between the low-tropospheric and the mid-tropospheric dynamics and their contributions to the thermal balance over EMED.

The nonlinear dynamical influences over EMED can be explored using the CTRL in order to differentiate impacts of the local (EMED) temperature on the local linkage between the mid- and upper tropospheric subsidence and surface circulation. Removing the time-varying climate forcing impacts from the HIST runs allows us to focus on the natural variability of the system and nonlinear interactions that may be difficult to statistically calculate in shorter HIST runs. As described in section 2, we construct two samples from the CTRL run with 300 July months with the lowest temperature and 300 with the highest one with respect to the mean surface temperature for the EMED region. We carry out a correlation analysis for these two periods, much as done in the previous section comparing recent historical and future periods. Figure SI7 shows a radical drop in derived correlations between the mid-level subsidence and the Mediterranean pressure, Etesian winds and their extension over the North Africa and Persian Gulf, and water vapor over the Sahel. These results are similar to those comparing present and future climate for these variables (Fig 11).

Figure 12 shows a direct response of the summer Mediterranean climate to the surface warming over EMED, estimated with composite differences between the two samples, in terms of temperature, relative humidity, pressure and wind vector, geopotential height at 500hPa and 800hPa, omega at 500hPa and precipitation. Interestingly, Figure 12a shows maximum of warming over Asia Minor and not the Levant, suggesting a potential feedback between these regions. Fig 12c shows bipolar SLP anomalies, with low pressure coincident with intensified heat low anomalies over North Africa, EMED and Middle East, and an anomalous anticyclonic circulation between northeast and northwest of this region. The latter is centered over the Black Sea and spreads towards the central Mediterranean, creating a stronger zonal pressure gradient over the Mediterranean and intensified Etesian winds. The intensified heat low over the EMED and Arabian Peninsula (Fig 12c) agree well with the enhanced local convergence and reduced subsidence at the low- and mid-tropospheric levels at 500hPa (Figure 12e) and 700hPa (not shown). At the same time, the positive SLP anomalies (Figure 12c) and increased subsidence over Asia Minor and Black Sea are physically consistent with increased adiabatic warming and stability, manifested in the local maximum warming, reduced relative humidity and precipitation. An analysis for the JJA season yields similar results, although with a reduced magnitude due to a smaller contribution of June and August months (Figure SI8).

Analysis of the effects of local warming over larger domains, i.e. including southern parts of the central and western Mediterranean (Figure SI9) yields similar results, i.e. opposite SLP anomalies for the southern Mediterranean (North Africa and the EMED) and northern central and eastern Mediterranean. However, the magnitude of the response over southwestern regions becomes equally strong to that over the EMED. Interestingly, analyses for regions which include the northeastern parts of the Mediterranean (30°-50°E, 30°-45°N), yields a reduced response (a weaker intensifying anticyclone) over these northern regions. Thus the derived anomalous anticyclone over Balkans and Black Sea is much stronger when the warming is confined to the southeastern parts (i.e. Levant and Arabian Peninsula). This emphasizes the role of the warming surface temperature over arid regions of North Africa and Arabian Peninsula in shaping the climate of the surrounding regions.

The composite response to anomalous warming over EMED can be readily associated with changes in the local circulation, i.e. an intensified zonal pressure gradient and Etesians over Mediterranean, as well as an intensified heat low, anomalous convergence and weakening low- and mid-tropospheric subsidence over the EMED and the Arabian Peninsula. All these changes are also seen in the future projections obtained for JJA (Figure 9a,b,c, Figure SI5a,c,e), and particularly in the month of July (Figure SI5b,d,f). Moreover, the response of positive SLP, increased subsidence and drying over central Mediterranean (i.e. Italy), the Balkan coast and Asia Minor are also consistent with the future changes (Figure 9), suggesting a potential contribution of the warming over Levant and the Arabian Peninsula to projected warming and drying over Asia Minor.

This analysis indicates that the dynamical regime over the EMED has a nonlinear influence on local temperature. During relatively cool years the dynamical relationship between the low-level circulation and mid-level subsidence, which balances the temperature over EMED, seems to be much stronger. By contrast, warming over EMED region can trigger a local response in the surface atmospheric circulation, which weakens the local dynamical linkages and hence their contribution in maintaining the local temperature balance. Hence it is possible that surface temperature-driven atmospheric responses will become a more prominent factor shaping future Mediterranean climate. This idea is supported by the consistency of this response (i.e. strong warming, intensifying heat low, anomalous convergence and very pronounced ascending motion at the low and mid-levels of the EMED and Arabian Peninsula, intensified zonal pressure gradient and Etesians, drying over Asia Minor and southern Balkans) with projected anthropogenic changes over the EMED region. Similar results are obtained for June and August, although with different intensity and location of the SLP and precipitation anomalies.

The analysis however does not explain the processes involved in the dipole-like response in the circulation, which includes SLP, winds and omega anomalies north from the EMED region (particularly Asia Minor and Black Sea). One might suspect that, in response to warming over the EMED, the anomalous convergence and ascending motion over the EMED triggers a seesaw connection with northward-located regions. This link could stem from the interactions of the anomalous warming and upward velocity anomalies with the seasonally varying descending branch of the Hadley cell over EMED, in result expanding it towards Asia Minor. Testing this hypothesis needs more elaborate analysis and could be objective of coming research.

5. Summary and Discussion

Based on the state of the art future projections (CMIP3 and CMIP5-generation) the Mediterranean has been identified as a climate change hot spot (Giorgi and Lionello 2008), not only due to the sensitivity of its climate to the anthropogenic forcing but also due to the socio-economic vulnerability of the local societies. Yet the projected changes are not fully reflected in the observations for the second half of the 20th century. While the derived anthropogenic fingerprint clearly suggests strong warming and drying during the summer, the observations indicate opposite wetting tendencies for some regions—in the vicinity of Black Sea and off the Balkan coast. This discrepancy may stem from the fact that the Mediterranean climate features abundant cross-scale variations, which at present dominate the anthropogenic signal. But there can be other reasons for this inconsistency, i.e. the deficiencies in models' representation of land-atmospheric feedbacks (as mentioned above) or the deficiencies in capturing impacts of certain teleconnections. The former has been shown to cause an overestimation of the projected future summer warming and drying in most of CMIP3 and CMIP5 models (Christensen and Boberg, 2012, Christensen and Boberg, 2012, Mueller and Seneviratne, 2014), particularly in the Mediterranean, Central and Southeast Europe (Diffenbaugh et al. 2007, Hirschi et al. 2011, Seneviratne et al., 2006). The latter has been suggested to incapacitate CMIP3/CMIP5 models in offsetting projected future regional drying, and hence spuriously exaggerate the regional warming and drying (Blade et al. 2012). The Mediterranean is a region of the confluence of the mid-latitude and subtropical teleconnections, which translated through the complex regional orography, makes simulating its climate extremely challenging. Obtaining realistic future projections for this region require not only refined spatial scales, but also a realistic balance between the contributing impacts of local land-atmosphere feedbacks, large-scale circulation, and teleconnections.

In this study, we use the high-resolution CM2.5 climate model integrations to analyze the projected regional future changes and interpret them through the prism of simulated SNAO teleconnections, the local dynamical regime, and the impact of warming land surface.

The analysis of the CM2.5 control run demonstrates the high capability of the model to simulate realistic summer climatology of the Mediterranean. The model very accurately reproduces key regional features of the associated large –scale atmospheric circulation, both in terms of the location and magnitude. This includes, for example, the subtropical mid-tropospheric anticyclone between the Levant and South Asia, and the low-tropospheric zonal pressure gradient between the subtropical North Atlantic anticyclone and the massive Asian monsoon heat low. The high spatial resolution of the integrations allows for capturing the sensitivity of the low-level atmospheric flow to the local orography, which is manifest in two branches of Etesian winds: over the Aegean Sea and its southward extension toward the Sahel region, as well as over the Persian Gulf. Also the mean precipitation, which features an exceptional spatial complexity in the Mediterranean, is represented with a much higher degree of realism when compared with the low-resolution CM2.1, for example.

Our analysis shows also that CM2.5 simulates teleconnection of the Mediterranean with the atmospheric circulation over the North Atlantic with high fidelity. The model plausibly reproduces the fingerprint of the summer North Atlantic oscillation (SNAO), and its influence on the Mediterranean hydroclimate, when compared with 20th century observations (Folland et al. 2009). Remarkably, the simulated (from the CTRL experiment_ SNAO fingerprint is in better agreement with the observed SNAO before the 1970s/1980s, rather than for the later decades. This is likely related to the strong multi-decadal signal of the SNAO in the most recent decades (as highlighted by Linderholm and Folland 2017) that may have partly originated from anthropogenic forcing, which is not included in the CM2.5 control run, though this is by no means certain. The impacts of the SNAO on the Mediterranean hydroclimate are comparable, in terms of pattern and magnitude, with the CMIP3/CMIP5 simulations, e.g. as manifested in the increased precipitation over

southern Europe during the positive SNAO phase. Overall, the analysis of the control run confirms the capability of CM2.5 to simulate key components of the regional climate, i.e. SNAO teleconnections and the local linkage between the surface and upper-level dynamics in the Mediterranean summer regime. The further analysis investigates the regional the future changes through the prism of future evolution of these two factors.

For the eastern Mediterranean, the most prominent features of its summer climate regime, i.e. the low-level northerly flow and the mid- and upper -tropospheric subsidence, are skillfully reproduced by the model. The strong linkage between these two factors demonstrates their counterbalancing effects on the regional temperature. Additionally, the significant correlations between the mid- and upper tropospheric subsidence over the Mediterranean and the indices of the Indian summer monsoon are consistent with the monsoon-desert mechanism (Rodwell and Hoskins, 1996, and Tyrlis et al., 2013).

The analysis of the CM2.5 projected future climate changes over the Euro-Atlantic region is to a large extent congruent with the CMIP5 ensemble. For example, changes in large-scale circulation over the North Atlantic, such as an expansion of the Hadley cell, an intensification and a northward shift of the atmospheric meridional cells, manifested by an anomalous anticyclone southwest of British Isles, constitute a typical fingerprint of the future summer anthropogenic change. In CM2.5, the general drying of the subtropics (southern Mediterranean) and wetting of the mid-latitudes (northern Europe) is consistent with the CMIP3/CMIP5 ensembles, and explained with the "wet-get-wetter and dry-get-drier" mechanism (Held and Soden, 2006; Seager et al., 2007). Consistent with previous CMIP studies, CM2.5 projects a much stronger warming in southwestern Europe and weaker warming in northeastern Europe.

However, CM2.5 projections reveal features, which are discernibly different from the CMIP3 and CMIP5 ensembles.For example, the magnitude of the CM2.5 projected warming over Europe and hence also the Mediterranean is much less radical. The derived future changes in precipitation over the Mediterranean are also smaller and feature a more complex pattern. This pattern consists of drying over large parts but also wetting tendencies over the Alps and northern parts of the Balkans. The CM2.5 projected wetting intensifies further towards central and northeastern Europe, which in contrast to CMIP3 and CMIP5 ensembles projecting rather drying over most of Europe, and wetting over Scandinavia. This difference is reflected in the projected in CM2.5 drying – wetting contrast over Europe, which is much sharper and with the transition zone being shifted southward, compared with the CMIP5 ensemble.

The CM2.5 projected future circulation over southern Europe also differs from the CMIP ensembles. CM2.5 projections indicate a strengthening of the zonal pressure gradient over the Mediterranean and the associated northerly flow/Etesian winds, contrary to a rather small weakening of the flow projected in CMIP5. This is a direct consequence of a) the strengthening anticyclonic circulation over the North Atlantic and higher sea level pressure over northwestern and central parts of Europe, and b) the intensification of the heat low over Sahara, the Persian trough and Asia Minor. In contrast, the intensified heat low in the CMIP5 ensemble covers not only arid subtropical regions but spreads over most of Eurasia (except the southern part of the monsoon region), suggestive of dominating contributions of land-atmosphere feedbacks.

Further analysis has shown also that the CM2.5 projected strengthening anticyclonic circulation over the North Atlantic is reflected in the strengthening of the SNAO towards its positive phase, which is also consistent with the CMIP3 and CMIP5 projections (e.g. Collins et al. 2013, Folland 2009). These changes of SNAO have been shown to be manifest in the positive anomalies of precipitation (wetting) over large parts of the Mediterranean. For example, without the impact of SNAO, the projected in CM2.5 drying over the Iberian

Peninsula, Italy, and the Balkan coast would be much stronger (locally up to ~30-40%). This confirms an important role of SNAO in counterbalancing the thermodynamic effects of the projected drying over the Mediterranean in both the CM2.5 and CMIP projections. Nevertheless, it is important to note that a) the representation of the regional SNAO impacts, and b) projected future changes in SNAO, is comparable between the CM2.5 and with some older generations models such as CM2.1, both in terms of pattern and magnitude. Thus SNAO does not seem to be a strong candidate explaining the differences in the future projections for the summer European climate between CM2.5 and CMIP3/CMIP5 ensembles.

Many studies have suggested rather that soil moisture-climate feedbacks are of dominant importance for summer climate in these regions (Seneviratne et al. 2006, Diffenbaugh 2007, Hirschi et al 2011). At the same time, most of CMIP3 and CMIP5 models are deficient in capturing soil moisture-atmosphere feedbacks (Christensen and Boberg, 2012; Mueller and Seneviratne, 2014, Boberg and Christensen, 2012). This causes a temperature dependent bias and spuriously amplifies the projected regional warming and drying, manifested ultimately in the CMIP5 ensemble mean as a very strong overall warming and drying over Europe. In contrast, Berg et al. 2016; Milly et al. 2014 demonstrated an improved representation of soil moisture and land-atmospheric feedbacks between soil moisture and precipitation in the LM3 model used in CM2.5. The enhanced feedbacks in this region are shown in Berg et al. (2015) with a lower resolution earth system model using LM3. Hence the apparent stark contrast between the CMIP3/CMIP5 and CM2.5 (mild warming and wetting) regional projections could more likely originate from the enhancements in the land model incorporated in CM2.5 at its high spatial resolution, rather than the impacts of the SNAO. These feedbacks should be explored in future work using targeted experiments like the Global Land–Atmosphere Coupling Experiment (Seneviratne et al. 2013) but lie outside the scope of this paper.

Additionally, the changes in climate regime projected in CM2.5 also suggest a weakening role of atmospheric dynamics in maintaining the regional hydroclimate and temperature balance over the eastern Mediterranean. For example, the projected changes over Asia Minor show very strong drying and warming, despite the increasing influence (i.e. wetting and cooling) of the SNAO teleconnection. Also, the warming over the Asia Minor and Levant regions constitutes a local maximum for the changes in the Mediterranean region, despite the cooling effect of strongly intensifying Etesians and the weakening mid- and upper-tropospheric subsidence in EMED.

The derived weakening linkage between the low-level circulation (e.g. northerly flow) and the mid-and upper-level subsidence over the EMED, which balances the regional temperature, is indicative of the nonlinearity in the summer EMED regime introduced by the local surface temperature. Additionally, the comparison of warmer and cooler EMED seasons in the control run indicates an increasing influence of local surface temperature on the local low-level atmospheric circulation in a warmer climate. This response stems likely from a sensitivity of this desert-like land to radiative forcing. It is manifest in an anomalous intensification of the heat low over the EMED, Sahara and the Persian trough, but also in positive SLP anomalies, increasing subsidence, maximum warming, reduced relative humidity, and reduced precipitation in the regions located north from Levant, in particular Asia Minor. All of these features are consistent with future climate changes projected by CM2.5. This supports the overall notion of an increasing impact of the interactions between land surface and atmosphere, as well as a decreasing influence of atmospheric dynamics, and hence of teleconnections, on the future summer regime in this region.

"The authors declare that they have no conflict of interest."

Acknowledgements

The authors are grateful to Ileana Blade, Fred Kucharski and Eduardo Zorita, Salvatore Pascale and Baoqiang Xiang for helpful comments and discussions.

References:

Alessandri, A., De Felice, M., Zeng, N., Mariotti, A., Pan, Y., Cherchi, A., Lee, J.Y., Wang, B., Ha, K.J., Ruti, P., Artale, V.: Robust assessment of the expansion and retreat of Mediterranean climate in the 21st century. Sci Rep 4:7211, 2014

Allan, R. and C.K. Folland, 2018: Atmospheric circulation. 1. Mean sea level pressure and related modes of variability—In: State of the Climate 2017. *Bull. Amer. Meteor. Soc*., **99**, S39-S41.

Alpert, P., Osetinsky, I., Ziv, B., Shafir, H.: A new seasons definition based on classified daily synoptic systems: an example for the eastern Mediterranean. Int J Climatol 24:1013–1021, 2004.

Baines, P. and C.K. Folland**,** 2007: Evidence for a rapid global climate shift across the late 1960s. *J. Climate,* **20,** 2721-2744.

Barcikowska, M., Knutson, T. and Zhang, R.: Observed and simulated fingerprints of multidecadal climate variability, and their contributions to periods of global SST stagnation. Journal of Climate, 30(2), 2017

Barcikowska, M., Kapnick, S.B., and F. Feser: Impact of large-scale circulation changes in the North Atlantic sector on the current and future Mediterranean winter hydroclimate. Climate Dynamics, 2017b, doi:10.1007/s00382-017-3735-5

Barnston, A.G., Livezey, R.E.: Classification, seasonality and persistence of low-frequency atmospheric circulation patterns. Mon Wea Rev 115:1083–1126, 1987

Berg, A., B.R. Lintner, K. Findell, S.I. Seneviratne, B. van den Hurk, A. Ducharne, F. Chéruy, S. Hagemann, D.M. Lawrence, S. Malyshev, A. Meier, and P. Gentine, 2015: Interannual Coupling between Summertime Surface Temperature and Precipitation over Land: Processes and Implications for Climate Change. J. Climate, 28, 1308–1328, https://doi.org/10.1175/JCLI-D-14-00324.1

Berg, A., Findell, K., Lintner, B., Giannini, A., Seneviratne, S. I., Van den Hurk, B., Ruth Lorenz, Andy Pitman, Stefan Hagemann, Arndt Meier, Frédérique Cheruy, Agnès Ducharne, Sergey Malyshev & P. C. D. Milly, 2016: Land–atmosphere feedbacks amplify aridity increase over land under global warming. Nature Climate Change, 6(9), 869.

Blade, I., Liebmann, B., Fortuny, D., van Oldenborgh, G.J.: Observed and simulated impacts of the summer NAO in Europe: implications for projected drying in the Mediterranean region. Clim Dyn 39:709–727, 2012.

Bladé, I., D. Fortuny, van Oldenborgh, G.J., Liebmann, B.: The summer North Atlantic Oscillation in CMIP3 models and related uncertainties in projected summer drying in Europe, J. Geophys. Res., 117, D16104, 2012b

Bitan, A., Saaroni, H.: The horizontal and vertical extension of the Persian Gulf pressure trough. Int J Climatol 12:733–747, 1992

Booth, B.B.B., Dunstone, N.J., Halloran, P.R., Andrews, T., and N. Bellouin, 2012: Aerosols implicated as a prime driver of twentieth-century North Atlantic climate variability, *Nature*, **484**, 228–232 doi:10.1038/nature10946

Cassou, C., L. Terray, J. W. Hurrell, and C. Deser: North Atlantic winter climate regimes: Spatial asymmetry, stationarity with time, and oceanic forcing. J. Climate, 17, 1055–1068, 2004

Cassou, C., L. Terray, and A. S. Phillips: Tropical Atlantic influence on European heat waves. J. Climate, 18, 2805–2811, 2005

Cherchi, A., Annamalai, H., Masina, S., Navarra, A.: South Asian summer monsoon and eastern Mediterranean climate: the monsoon- desert mechanism in CMIP5 simulations. J Clim 27: 6877– 6903, 2014

Cherchi, A., Annamalai, H., Masina, S. et al. Clim Dyn (2016) 47: 2361. https://doi.org/10.1007/s00382-015-2968-4

Cheruy, F., J. L. Dufresne, F. Hourdin, and A. Ducharne: Role of clouds and land -atmosphere coupling in midlatitude continental summer warm biases and climate change amplification in CMIP5 simulations, Geophys. Res. Lett., 41, 6493–6500, doi:10.1002/2014GL061145, 2014.

Christensen, J. H., and F. Boberg: Temperature dependent climate projection deficiencies in CMIP5 models, Geophys. Res. Lett., 39, L24705, doi:10.1029/2012GL053650, 2012.

Chronis, T., Raitsos, D.E., Kassis, D., Sarantopoulos, A.: The summer North Atlantic oscillation influence on the Eastern Mediterranean.J Clim 24:5584–5596, 2011

Collins, M., R. Knutti, J. Arblaster, J.-L. Dufresne, T. Fichefet, P. Friedlingstein, X. Gao, W.J. Gutowski, T. Johns, G. Krinner, M. Shongwe, C. Tebaldi, A.J. Weaver and M. Wehner, 2013: Long-term Climate Change: Projections, Commitments and Irreversibility. In: Climate Change 2013: The Physical Science Basis. Contribution of Working Group I to the Fifth Assessment Report of the Intergovernmental Panel on Climate Change [Stocker, T.F., D. Qin, G.-K. Plattner, M. Tignor, S.K. Allen, J. Boschung, A. Nauels, Y. Xia, V. Bex and P.M. Midgley (eds.)]. Cambridge University Press, Cambridge, United Kingdom and New York, NY, USA.

Compo, G.P., J.S. Whitaker, and P.D. Sardeshmukh, 2006: Feasibility of a 100 year reanalysis using only surface pressure data. Bull. Amer. Met. Soc., 87, 175-190, http://dx.doi.org/10.1175/BAMS-87-2-175.

Compo, G.P., J. S. Whitaker, P. D. Sardeshmukh, N. Matsui, R. J. Allan, X. Yin, B. E. Gleason Jr., R. S. Vose, G. Rutledge, P. Bessemoulin, S. Brönnimann, M. Brunet, R. I. Crouthamel, A. N. Grant, P. Y. Groisman, P. D. Jones, M. C. Kruk, A. C. Kruger, G. J. Marshall, M. Maugeri, H. Y. Mok, Ø. Nordli, T. F. Ross, R. M. Trigo, X. L. Wang, S. D. Woodruff, S. J. Worley, 2011: The twentieth century reanalysis project. Q. J. R. Meteorol. Soc. 137, 1–28.

Cornes, R., G. van der Schrier, E.J.M. van den Besselaar, and P.D. Jones. 2018: An Ensemble Version of the E-OBS Temperature and Precipitation Datasets, J. Geophys. Res. Atmos., **123**. doi:10.1029/2017JD028200

Delworth, T.L., A.J. Broccoli, A. Rosati, R.J. Stouffer, V. Balaji, J.A. Beesley, W.F. Cooke, K.W. Dixon, J. Dunne, K.A. Dunne, J.W. Durachta, K.L. Findell, P. Ginoux, A. Gnanadesikan, C.T. Gordon, S.M. Griffies, R. Gudgel, M.J. Harrison, I.M. Held, R.S. Hemler, L.W. Horowitz, S.A. Klein, T.R. Knutson, P.J. Kushner, A.R. Langenhorst, H. Lee, S. Lin, J. Lu, S.L. Malyshev, P.C. Milly, V. Ramaswamy, J. Russell, M.D. Schwarzkopf, E. Shevliakova, J.J. Sirutis, M.J. Spelman, W.F. Stern, M. Winton, A.T. Wittenberg, B. Wyman, F. Zeng, and R. Zhang, GFDL's CM2 Global Coupled Climate Models. Part I: Formulation and Simulation Characteristics. *J. Climate,* 19, 643–674, 2006

Delworth, T.L., A. Rosati, W. Anderson, A.J. Adcroft, V. Balaji, R. Benson, K. Dixon, S.M. Griffies, H. Lee, R.C. Pacanowski, G.A. Vecchi, A.T. Wittenberg, F. Zeng, and R. Zhang, 2012: Simulated Climate and Climate Change in the GFDL CM2.5 High-Resolution Coupled Climate Model. *J. Climate,* 25, 2755–2781, 2012

Delworth, T. and Mann, M.: Observed and simulated multidecadal variability in the Northern Hemisphere Climate Dynamics, 16: 661, 2000

Diffenbaugh, N. S., J. S. Pal, F. Giorgi, and X. Gao: Heat stress intensification in the Mediterranean climate change hotspot, Geophys. Res. Lett., 34, L11706, doi:10.1029/2007GL030000, 2007

Enfield, D. B., Mestas‐Nunez, A.M., Trimble, P.J.: The Atlantic multidecadal oscillation and its relation to rainfall and river flows in the continental U.S., Geophys. Res. Lett., 28, 2077–2080, 2001

Fontaine, B. , Roucou, P. , Gaetani, M. and Marteau, R. (2011), Recent changes in precipitation, ITCZ convection and northern tropical circulation over North Africa (1979–2007). Int. J. Climatol., 31: 633-648. doi:10.1002/joc.2108

Giorgi, F. ; 2006: Climate change hot‐spots, Geophys. Res. Lett., 33, L08707, doi:10.1029/2006GL025734.

Giorgi, F. and Lionello, P.: Climate change projections for the Mediterranean region. Glob Planet Change 63:90–104, 2008

Feng, S., Hu, Q., Huang, W., Ho, C.-H., Li, R. & Tang, Z. Projected climate regime shift under future global warming from multi-model, multi-scenario CMIP5 simulations. Global Planet. Change 112, 41–52 (2014).
Füssel, H.M., André Jol, Andreas Marx, et al. edited by Hans-Martin Füssel, André Jol, Andreas Marx, Mikael Hildén: Climate change, impacts and vulnerability in Europe 2016 - An indicator-based report Vol. 1/2017.

Folland, C.K., Knight, J., Linderholm, H.W., Fereday, D., Ineson, S., Hurrell, J.W.: The summer North Atlantic Oscillation: past, present, and future. J Climate 22:1082–1103, 2009

Hanf, F., Körper, J., Spangehl, T. & Cubasch, U. Shifts of climate zones in multi-model climate change experiments using the Köppen climate classification. Meteorol. Z. 21, 111–123 (2012).

Hoskins, B.J.,: On the existence and strength of the summer subtropical anticyclones —Bernhard Haurwitz memorial. Bull Am Meteorol Soc 77:1287–1292, 1996

HMSO: Weather in the Mediterranean I: general meteorology, 2nd edn. Her Majesty Stationery Office, London, p 362, 1962

Hurrell, J.W.: Decadal trends in the North Atlantic Oscillation: regional temperatures and precipitation. Science 269:676–679, 1995

Hurrell, J.W., Deser, C.: North Atlantic climate variability: the role of the North Atlantic Oscillation. J Mar Syst 78(1): 28–41, 2009

Hurrell, J.W., Folland, C.K.: A change in the summer circulation over the North Atlantic. CLIVAR Exchanges, No. 25, International CLIVAR Project Office, Southampton, United Kingdom, pp 52–54, 2002

Hurrell, J.W., Kushnir, Y., Ottersen, G., Visbeck, M.: An overview of the North Atlantic Oscillation. The North Atlantic Oscillation: climatic significance and environmental impact. Geophys Monogr. Am Geophys Union 134:1–35, 2003

Hurrell, J. W., and H. van Loon: Decadal variations in climate associated with the North Atlantic Oscillation. Climatic Change, 36, 301–326, 1997

Jacob, D., Petersen, J., Eggert, B., Alias, A., Christensen, O. B., Bouwer, L. M., Braun, A., Colette, A., Déqué, M., Georgievski, G., Georgopoulou, E., Gobiet, A., Menut, L., Nikulin, G., Haensler, A., Hempelmann, N., Jones, C., Keuler, K., Kovats, S. et al., 2014, 'EURO-CORDEX: New high-resolution climate change projections for European impact research', Regional Environmental Change 14(2), 563–578 (doi: 10.1007/s10113-013-0499-2).

Kalnay et al.,The NCEP/NCAR 40-year reanalysis project, Bull. Amer. Meteor. Soc., 77, 437-470, 1996.

Kanamitsu, M., W. Ebisuzaki, J. Woollen, S. Yang, J.J. Hnilo, M. Fiorino, and G.L. Potter: NCEP–DOE AMIP-II Reanalysis (R-2). *Bull. Amer. Meteor. Soc.,* 83, 1631–1644, 2002

Kelley, C., Ting, M., Seager, R., Kushnir, Y.: Mediterranean precipitation climatology, seasonal cycle, and trend as simulated by CMIP5. Geophys Res Lett 39:L21703, 2012

Krichak, S.O., Kishcha, P., Alpert, P.: Decadal trends of main Eurasian oscillations and the Mediterranean precipitation, Teor. Appl. Climatol., 72: 29-220, 2002

Knight, J. R., R. J. Allan, C. K. Folland, M. Vellinga, and M. E. Mann: A signature of persistent natural thermohaline circulation cycles in observed climate. Geophys. Res. Lett., 32, L20708, 2005

Knight, J. R., R., C. K. Folland, and A. A. Scaife, 2006: Climatic impacts of the Atlantic multidecadal oscillation. Geophys. Res. Lett., 33, L17706, doi:10.1029/2006GL026242

Legates, D. R., and C. J. Willmott, 1990: Mean seasonal and spatial variability in gauge-corrected, global precipitation. Int. J. Climatol.,10, 111–127.

Lelieveld, J., Berresheim, H., Borrmann, S., et al.: Global air pollution crossroads over the Mediterranean. Science 298: 794–799, 2002

Lelieveld, J., Hadjinicolaou, P., Kostopoulou, E., Chenoweth, J., Giannakopoulos, C., Hannides, C., Lange, M.A., El Maayar, M., Tanarthe, M., Tyrlis, E., Xoplaki, E.: Climate change and impacts in the eastern Mediterranean and the Middle East. Clim Chang 114:667–687, 2012

Lin, H.: Global extratropical response to diabatic heating variability of the Asian summer monsoon. J Atmos Sci 66: 2697–2713, 2009

Lin, H., Derome, J., Brunet, G.: The nonlinear transient atmospheric response to tropical forcing. J Clim 20:5642–5665, 2007

Linderholm, H.W. and C K. Folland, 2017: Summer North Atlantic Oscillation (SNAO) variability on interannual to palaeoclimate time scales. *CLIVAR Exchanges* **72,** 57-60 and *Past Global Changes Magazine,* 25, No. 1**.** doi: 10.22498/pages.25.1.57

Linderholm, H.W., Folland, C.K. and A. Walther, 2009: A multicentury perspective on the summer North Atlantic Oscillation (SNAO) and drought in the eastern Atlantic Region. *J. Quaternary Science*, **24,** 415-425. Doi:10.1002/jqs.1261

Maheras, P.: Le problem des Etesiens. Mediterranee, N40, 57-66, 1980.

Mann, M. E., and Emanuel, K.A.: Atlantic hurricane trends linked to climate change, *Eos Trans. AGU*, 87(24), 233–241, doi: 10.1029/2006EO240001, 2006

Mariotti, A., Dell'Aquila, A.: Decadal climate variability in the Mediterranean region: roles of large-scale forcings and regional processes. Clim Dyn 38:1129–1145, 2012

Mariotti, A., Pan, Y., Zeng, N., Alessandri, A.: Long-term climate change in the Mediterranean region in the midst of decadal variability. Clim Dyn 44:1437–1456, 2015

Mariotti, A., Struglia, M.V., Zeng, N., Lau, K.M.: The hydrological cycle in the Mediterranean region and implications for the water budget of the Mediterranean Sea. J Clim 15:1674–1690, 2002

Meehl, G., A. et al. Global climate projections. In: Solomon S et al. (eds) Climate change 2007: The Physical Science Basis. Cambridge University Press, Cambridge, pp 747–845, 2007.

Meinshausen, M. and Smith,J. S and Calvin, K.V. and Daniel, J., and Kainuma, M., and Lamarque, J.-F. and Matsumoto, K., and A Montzka, S., C B Raper, S., and Riahi, K. and Thomson, A.M. and Velders, Guus J. M., and Vuuren, D: The RCP greenhouse gas concentrations and their extensions from 1765 to 2300. Climatic Change, 2011

Metaxas D.A: The interannual variability of the Etesian frequency as a response of atmospheric circulation anomalies. Bulletin of the Hellenic Meteorological Society 2(5): 30–40, 1977

Milly, P.C., S.L. Malyshev, E. Shevliakova, K.A. Dunne, K.L. Findell, T. Gleeson, Z. Liang, P. Phillipps, R.J. Stouffer, and S. Swenson, 2014: An Enhanced Model of Land Water and Energy for Global Hydrologic and Earth-System Studies. J. Hydrometeor., 15, 1739–1761, https://doi.org/10.1175/JHM-D-13-0162.1

Mueller, B., and S. I. Seneviratne (2014), Systematic land climate and evapotranspiration biases in CMIP5 simulations, Geophys. Res. Lett., 41, 128–134, doi:10.1002/2013GL058055, 2014.

Mueller, B., and S. I. Seneviratne (2012), Hot days induced by precipitation deficits at the global scale, Proc. Natl. Acad. Sci. U. S. A., 109, 12,398–12,403, doi:10.1073/pnas.1204330109, 2012.

Prezerakos, N.G.: Does the extension of the Azores anticyclone towards the Balkans really exist. Archive fur Meteorologie, Geophysile und Bioklimatologie, Serie A: Meteorologie und Geophysik 33: 217–227, 1984

Poli, P., H. Hersbach, P. Berrisford, and coauthors: ERA-20C Deterministic. ERA Report Series Number 20, 2015

Riahi, K., Rao, S., Krey, V. et al. Climatic Change, 109: 33. 2011

Raicich, F., Pinardi, N., Navarra, A.: Teleconnections between Indian monsoon and Sahel rainfall and the Mediterranean. Int J Climatol 23:173–186, 2003

Rizou, D., Flocas, H.A., Athanasiadis, P., Bartzokas, A.: Relationship between the Indian summer monsoon and the large-scale circulation variability over the Mediterranean, Atmospheric Research, Volume 152, 159-169, 2015.

Reddaway, J.M., Bigg, G.R.: Climatic change over the Mediterranean and links to the more general atmospheric circulation. Int J Climatol 16:651–661, 1996

Rodwell, M.J., Hoskins, B.J.: Monsoons and the dynamics of deserts. Q J R Meteorol Soc 122:1385–1404, 1996

Rodwell, M.J., Hoskins, B.J.: Subtropical anticyclones and summer monsoons. J Clim 14:3192–3211, 2001

Rotstayn, L., and U. Lohman: Tropical rainfall trends and the indirect aerosol effect. J. Climate, 15, 2103–2116, 2002

Rowell, D.P., 2003: The Impact of Mediterranean SSTs on the Sahelian Rainfall Season. J. Climate, 16, 849–862, https://doi.org/10.1175/1520-0442(2003)016<0849:TIOMSO>2.0.CO;2

Rowell, D.P. and Jones, R.G., 2006: Causes and uncertainty of future summer drying over Europe. Climate Dynamics, 27: 281-299

Saaroni, H., Ziv, B.: Summer rain episodes in a Mediterranean climate, the case of Israel: climatological-dynamical analysis. Int J Climatol 20:191–209, 2000

Saaroni, H., Ziv, B., Osetinsky, I., Alpert, P.: Factors governing the interannual variation and the long-term trend of the 850 hPa temperature over Israel. Q J R Meteorol Soc 136:305–318, 2010

Scaife, A., Folland, C.K., Alexander, L.V. Moberg, A., Brown, S. and J.R. Knigh*t,* 2008: European climate extremes and the North Atlantic Oscillation. *J. Climate***, 21**, 72-83.

Seneviratne, S. I., D. Lüthi, M. Litschi, and C. Schär: Landatmosphere coupling and climate change in Europe, Nature, 443(7108), 205–209, doi:10.1038/nature05095, 2006

Seneviratne, S. I., et al. : Changes in climate extremes and their impacts on the natural physical environment, in Managing the Risks of Extreme Events and Disasters to Advance Climate Change Adaptation. A Special Report of Working Groups I and II of the Intergovernmental Panel on Climate Change (IPCC), edited by C. B. Field et al., pp. 109–230, Cambridge Univ. Press, Cambridge, U. K, 2012

Sutton, R. T., and D. L. R. Hodson: Atlantic Ocean forcing of the North American and European summer climate. Science, 309, 115–118, 2005

Trenberth K.E., Paolino D.A. Jr: The Northern Hemisphere sea level pressure data set: trends, errors and discontinuities. Mon Wea Rev, 108:855–872, 1980

Tyrlis, E., Lelieveld, J., Steil, B.: The summer circulation over the Eastern Mediterranean and the Middle East: influence of the South Asian monsoon. Clim Dyn 40:1103–1123, 2013

Willmott, C. J. and K. Matsuura: Terrestrial Air Temperature and Precipitation: Monthly and Annual Time Series (1950 - 1999), 2001

Zecchetto, S., de Biasio, F.: Sea surface winds over the Mediterranean basin from satellite data (2000-04): meso- and local-scale features on annual and seasonal time scales. J Appl Meteorol Climatol 46:814–827, 2007

Ziv, B., Saaroni, H., Alpert, P.: The factors governing the summer regime of the eastern Mediterranean. Int J Climatol 24:1859–1871, 2004

Table1 Abbreviation names for the CM2.5 experiments

NAME of the experiment	**Ensemble size**	**Number of years total**	**Historical period [yrs]**
CTRL	1	1000 yrs	-
HIST	5	145	1861-2005
PROJ	5	95	2006-2100

FIGURES

Figure 1. Seasonal (JJA) sea level pressure (hPa) and wind vector at 850hPa (m/s) in a) NCEP-DOE2, b) CM2.5. Time-mean of seasonal data from years 101–1000 of the control simulations are used, and years 1979-2017 of the observed data.

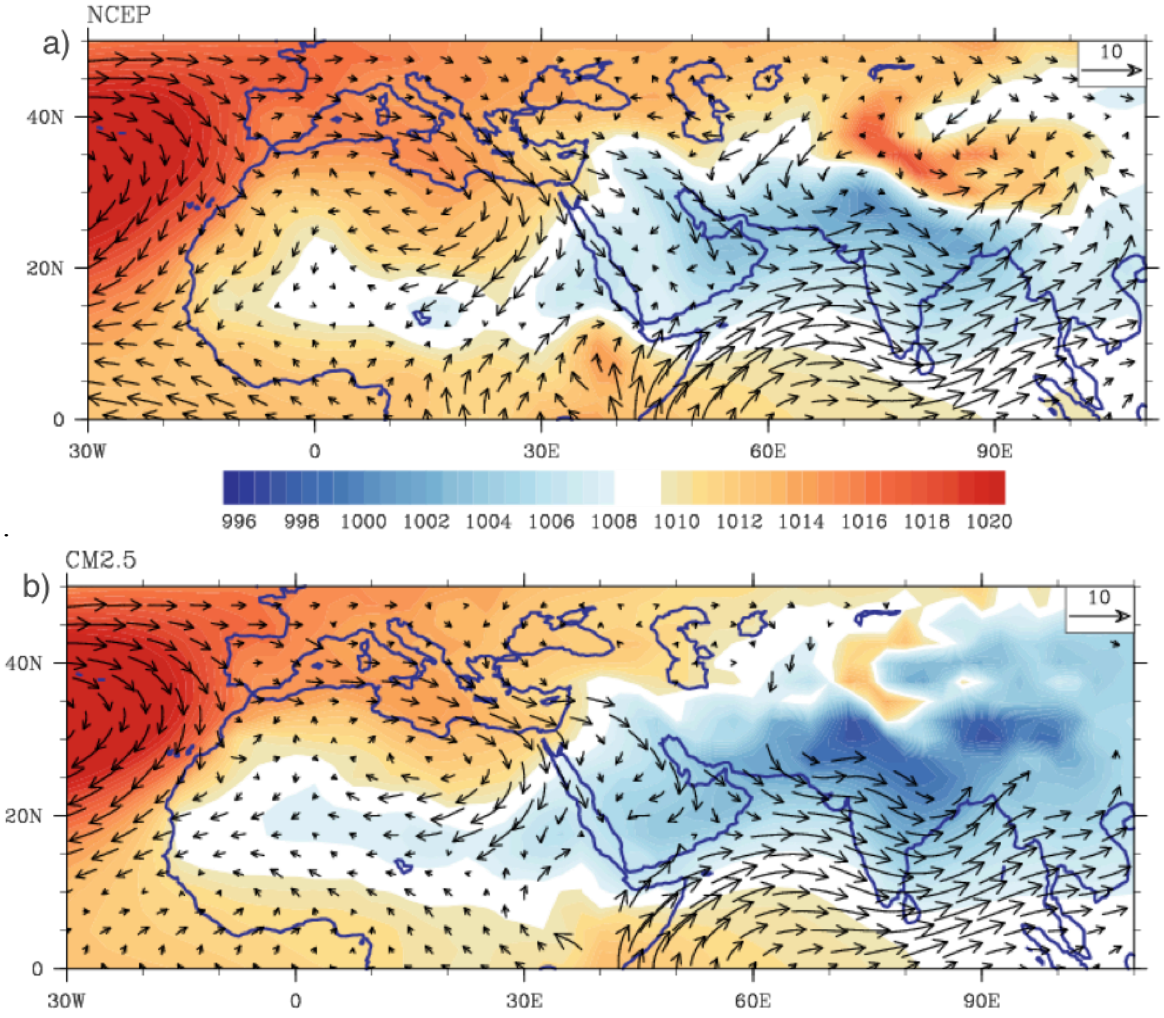

Figure 2. Seasonal (July) time-mean vertical velocities at 500hPa (Pa/s) and wind vectors at 200hPa (Pa/s), estimated for a) NCEP-DOE2 in the period 1979-2017, and b) CM2.5 CTRL run in years 101-1000. Both data sets are interpolated to the 2.5° horizontal grid.

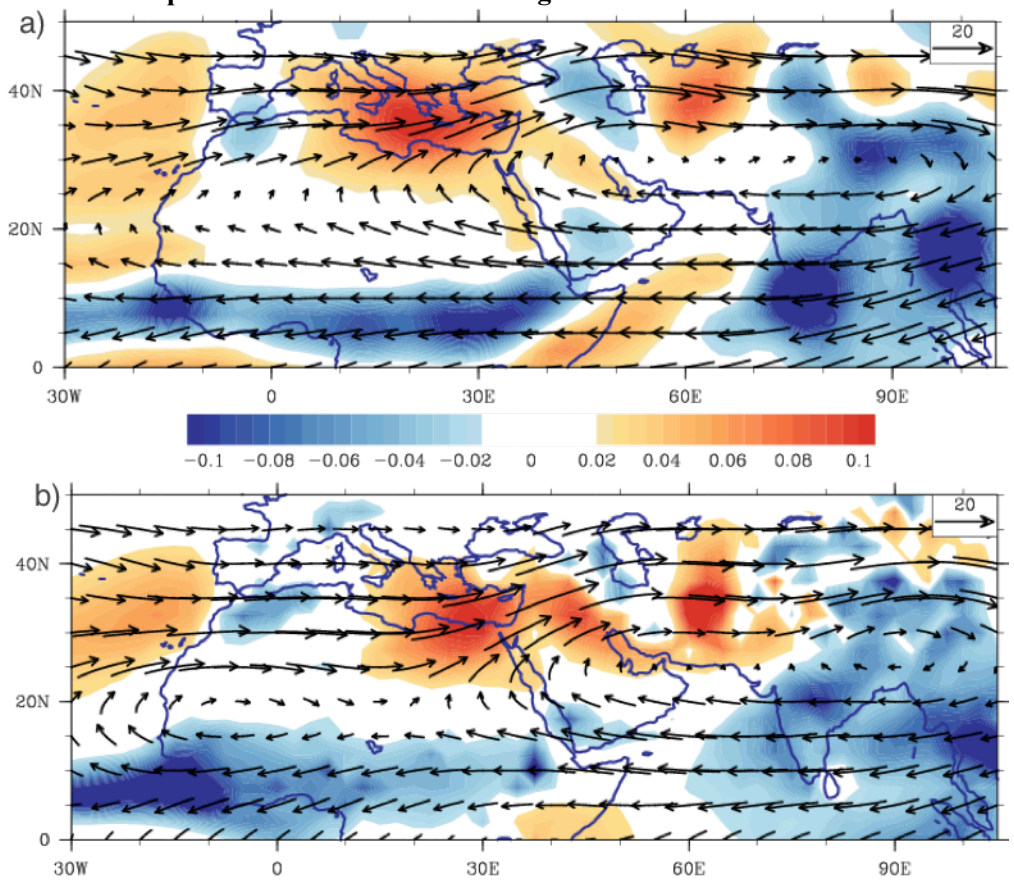

Figure 3. Height (pressure)-longitude cross-section of vertical velocity (Pa/s, shaded contours, downward motion denoted with positive values) and vector of zonal wind (m/s) and vertical velocity (converted to m/s and scaled with a factor of 1000) in July. Figure shows time-mean values in July a) derived for the period 1979-2017 in NCEP-DOE2, b) derived from 101-1000 years of CNTL run in CM2.5; and c) projected future changes in the period 2061-2099 in PROJ ensemble mean, compared with the baseline period 1961-1999 in the HIST ensemble mean. All fields are shown on the 2.5°x2.5° horizontal grid and at the original vertical levels, common for CM2.5 and NCEP-DOE2.

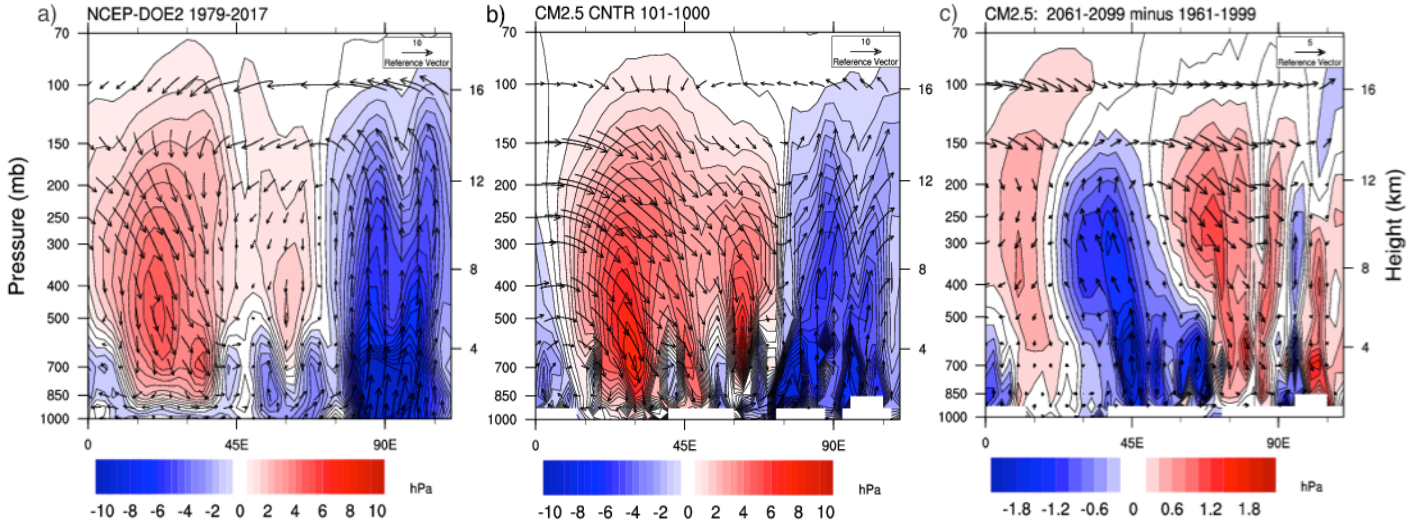

Figure 4. Seasonal (JJA) mean precipitation (mm/day) for a) EOBS observations, b) University of Delaware Climatology, b) CM2.1, c) CM2.5. The time-mean of seasonal data from years 101–1000 of the control simulations are used, and years 1980-2015 of the observed data sets. Both observational data sets are shown at 0.5° lat x lon resolution. Regions with missing data are left blank.

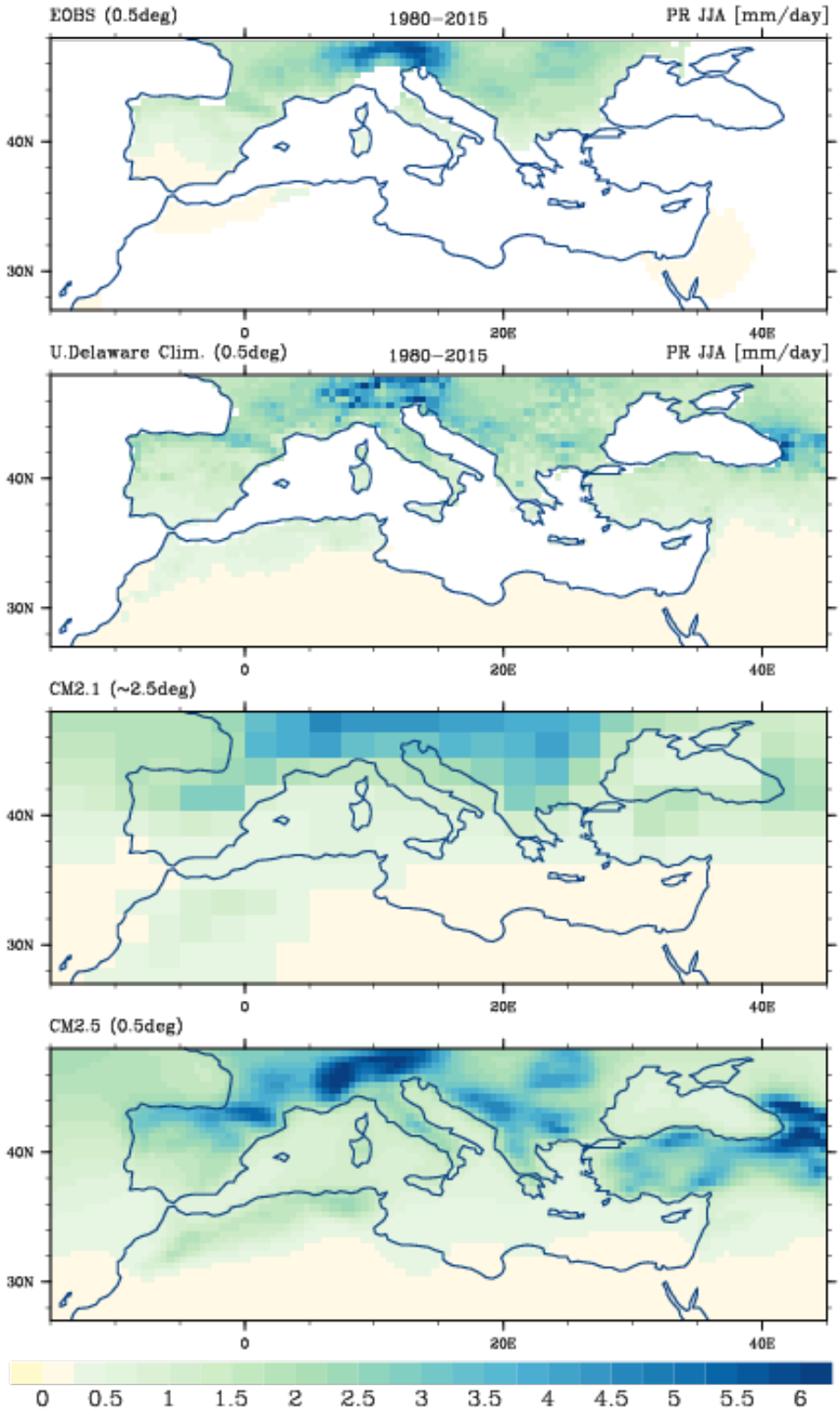

Figure 5. Correlation between principal component time series of the SNAO SLP in JA and a) sea level pressure b) temperature at 2m (shaded) and geopotential height at 850hPa (contours), c) precipitation. All derived from the CTRL run. Contours in a) and c) are shown for 0.25 and 0.5 correlations. Correlations are shown only when significant at 1% level.

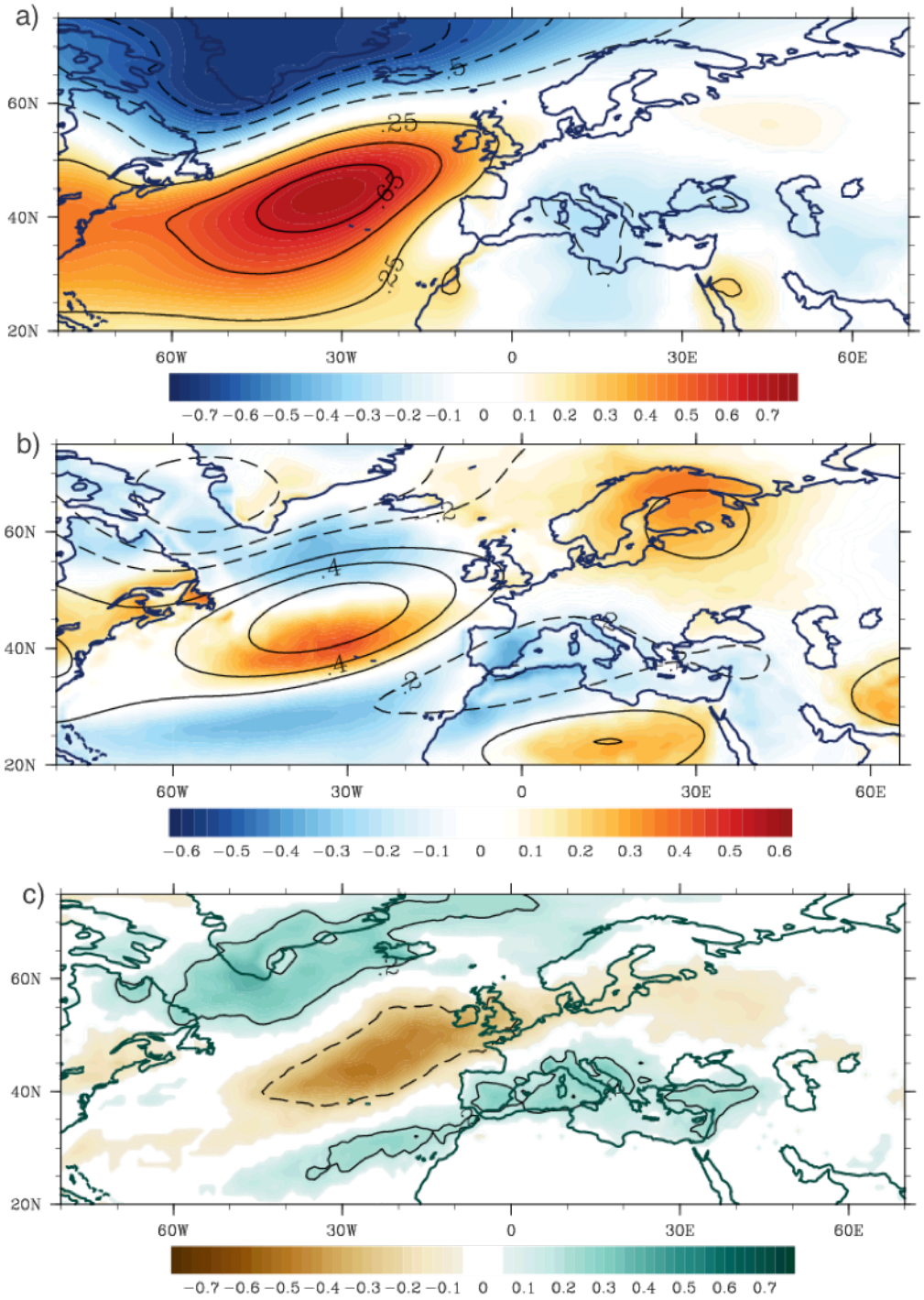

Figure 6. Spatial pattern of the SNAO (EOF), derived from the 20CR reanalysis (left), and from the first CM2.5 HIST run (right), shown as correlations between the first principal component time series and SLP in July-August. The pattern is derived from periods a)-b) 1870-1920, c)-d) 1900-1950, e)-f) 1940-1990, g)-h) 1960-2010. Please note that the sign of each derived EOF is arbitrary. The analysis took into account that fact and unified the sign, showing the SNAO at its positive phase.

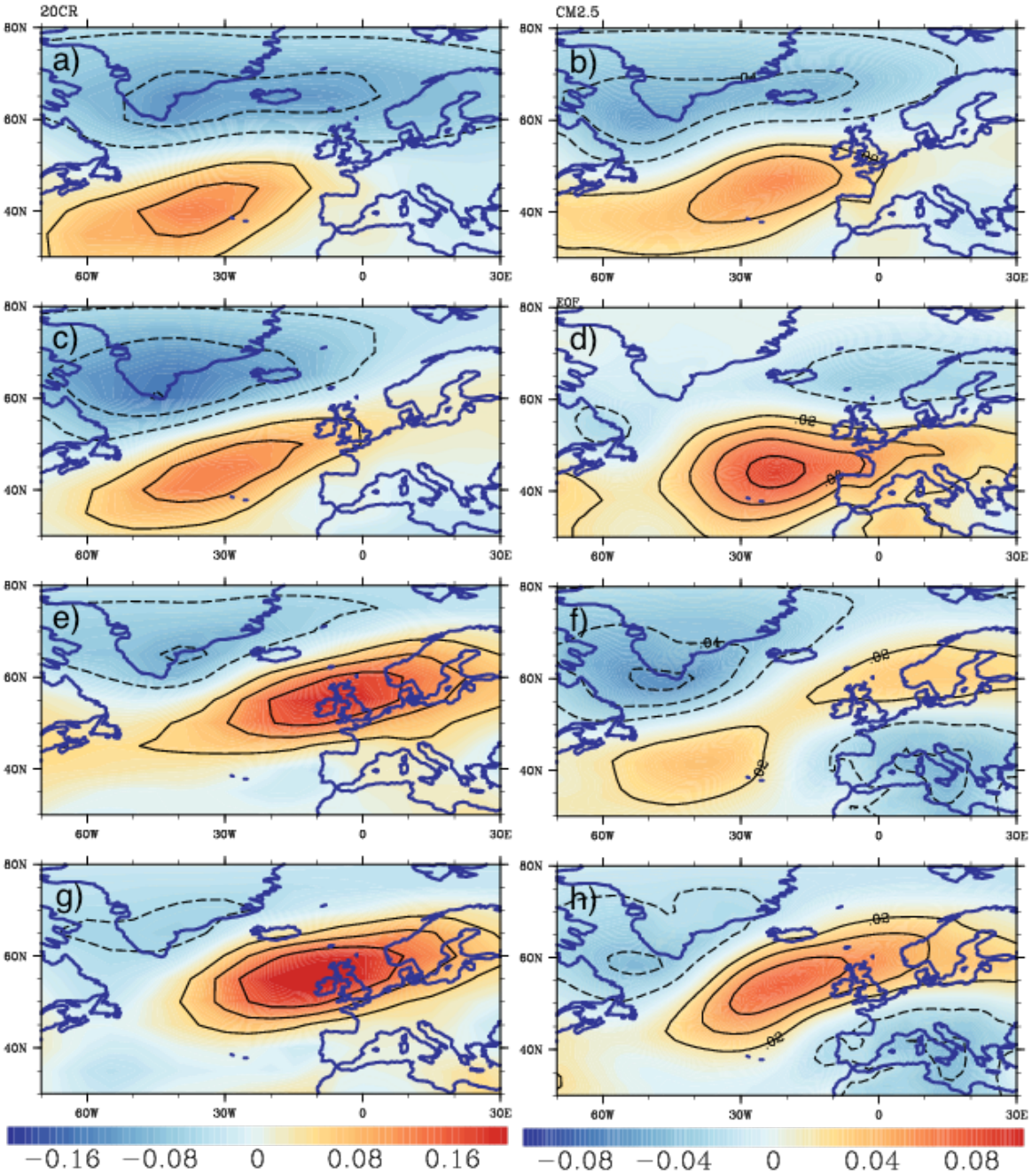

Figure 7. a) First EOF of CM2.5 vertical velocities at 500 hPa (EOF1 omega, shaded) and 300hPa (contours), derived from the monthly mean of July in the CTRL run. The time series of EOF1 omega at 500 hpa are correlated with b) geopotential height (shaded), u, v components (shown as vector) at 850hPa and c) meridional wind at 850hPa. d) Correlations derived between the observed (NCEP) omega 500hPa over the eastern Mediterranean region (32°-34°N, 25°-30°E) and the meridional wind at 850hPa. Correlations shown are at b)-c) the 1%, and d) the 10% significance level.

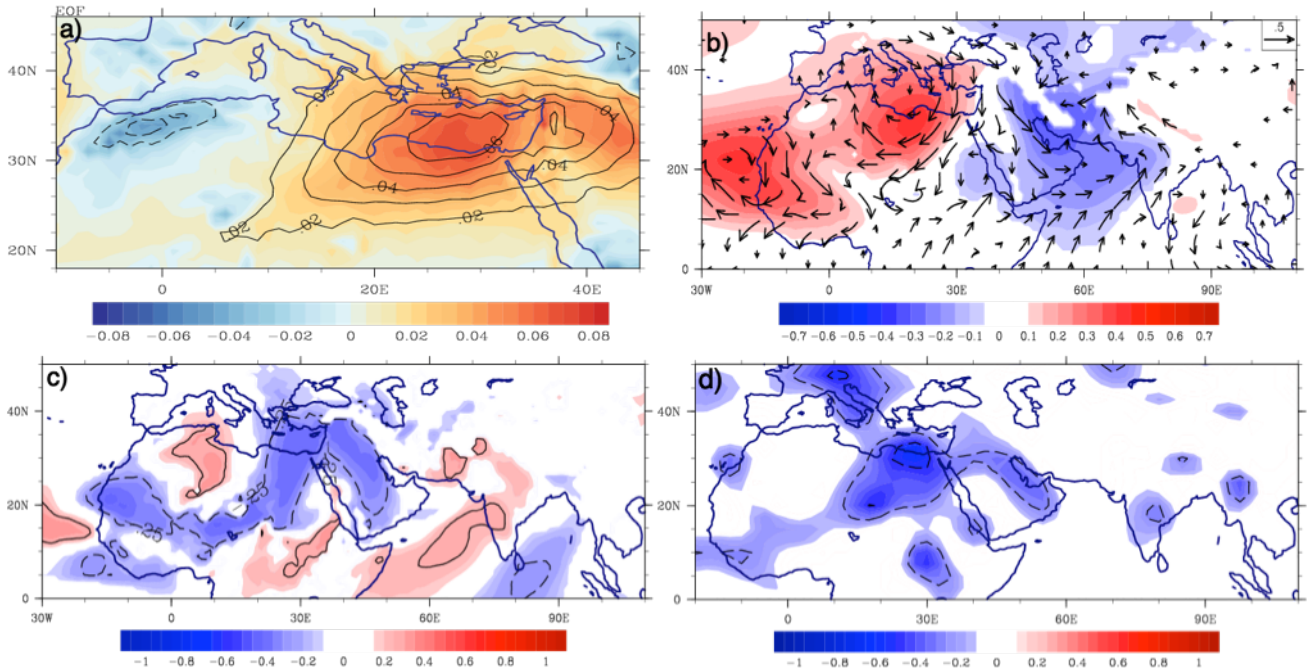

Figure 8. Correlations between the time series of the EOF1 omega (derived for omega 500hPa, see Figure 7a) and a) outgoing long wave radiation (shaded), omega at 500 hPa (contours: -0.2, 0.2, 0.4), b) precipitation; derived from the monthly means of July in CTRL run. Correlations shown are at the 1% significance level.

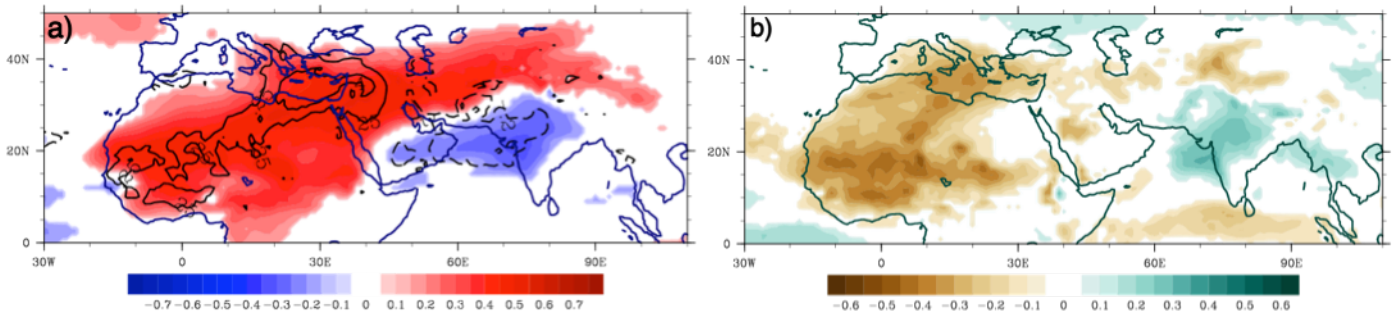

Figure 9. Projected future changes for the summer (JJA) a) sea level pressure (hPa, shaded) and u,v wind components at 850hPa (m/s, vector), b) surface temperature (°C), c) total precipitation rate [mm/day], over the period 2061-2099 compared with the baseline period 1961-1999. Changes are derived at the original horizontal resolution.

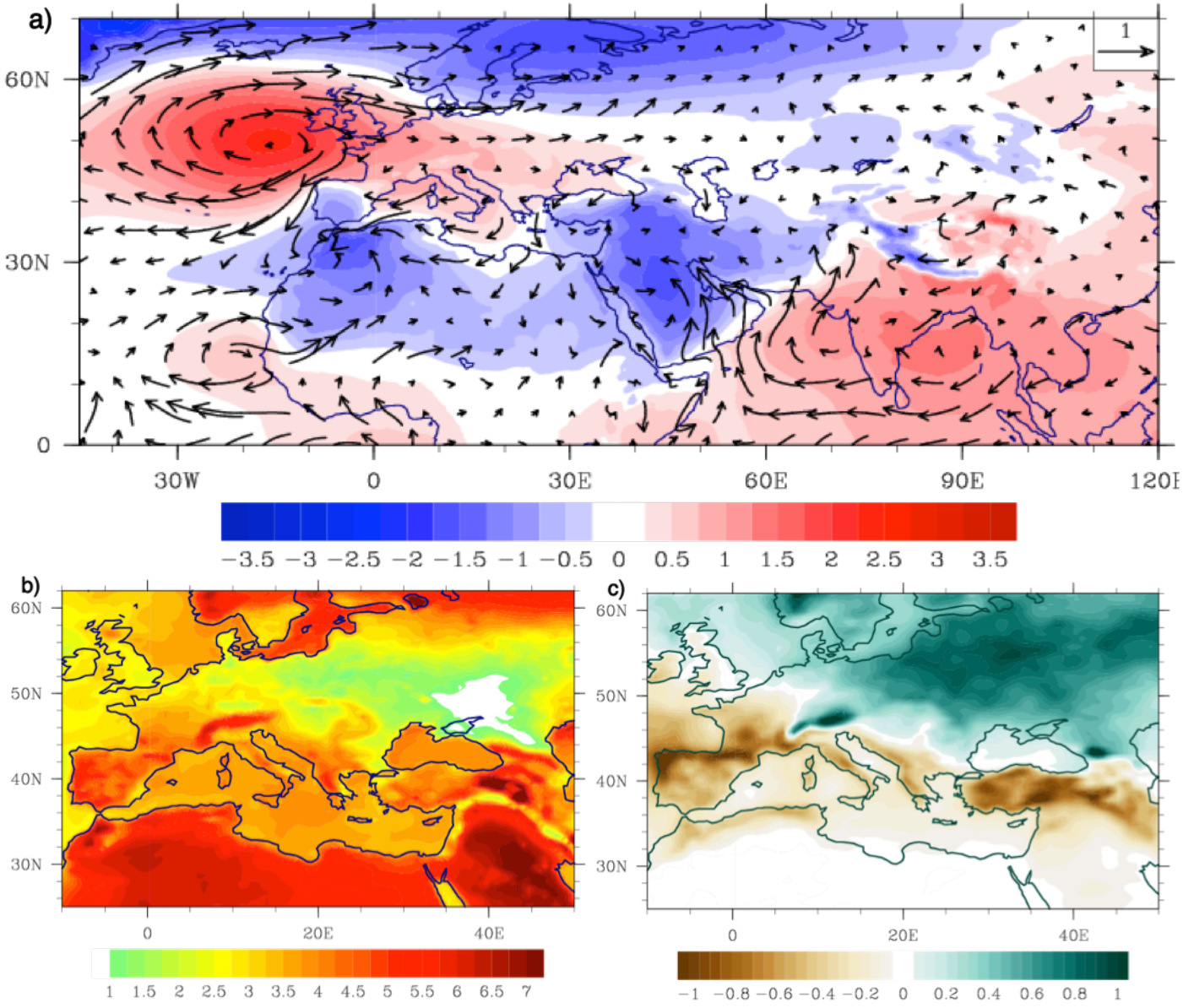

Figure 10. (a, b) Correlations (shaded) between the SNAO time series and precipitation in1900-1950 (a) HIST runs), and 2050-2100 (b) PROJ runs). Contours denote 0.25 and 0.5. c) Evolution of SNAO SLP time series in 1850-2100 period for each run (blue) and the ensemble mean (red). The vertical line divides the HIST and PROJ time series. (d, e) Projected future changes in the summer precipitation (mm/day) (as in Fig 8c, except that estimated at 1° horizontal resolution), d) including SNAO impact and e) with the impact of the future SNAO removed (shaded). The impact of SNAO is estimated based on the linear regression between the detrended time series of SNAO and precipitation.

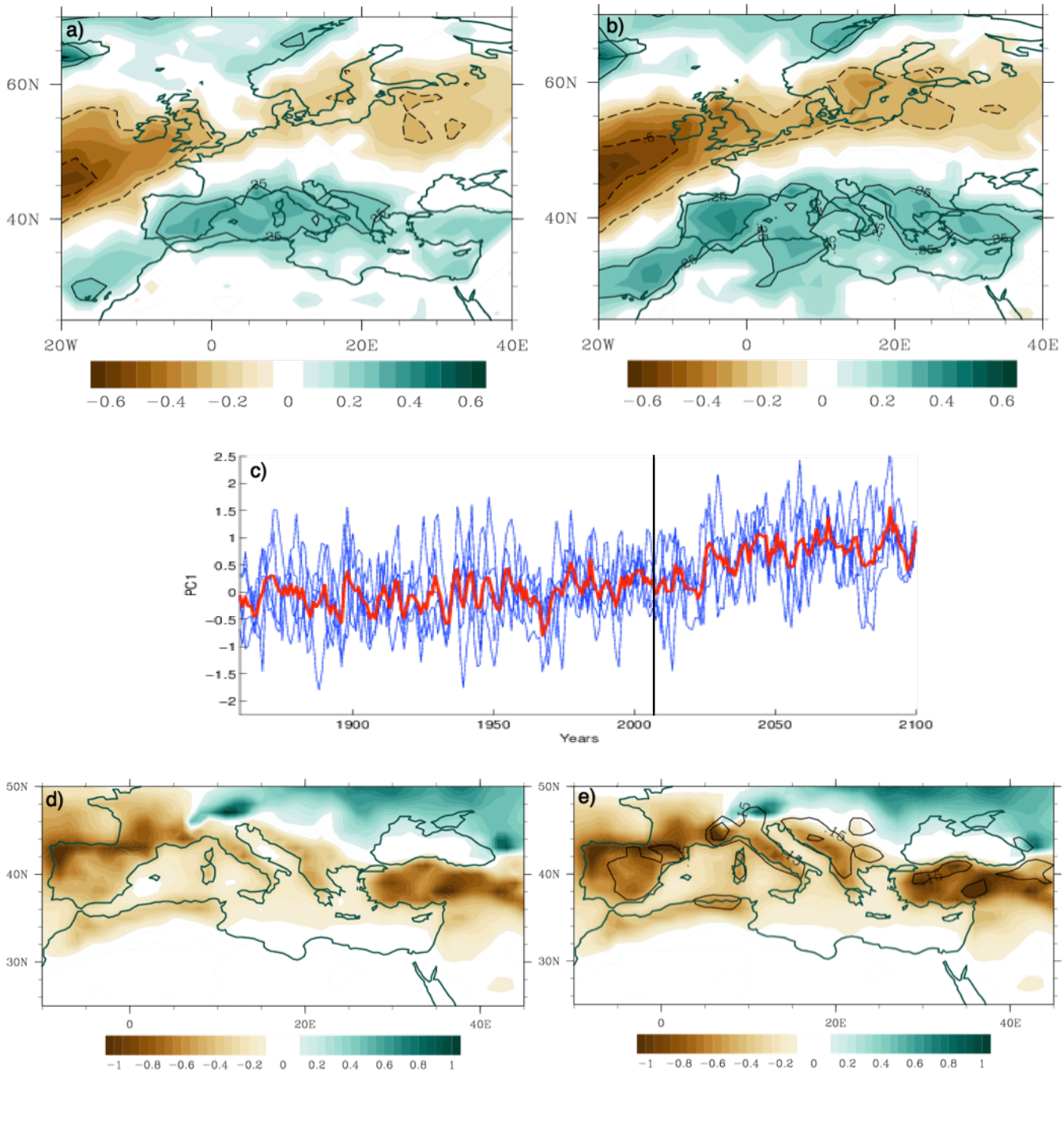

Figure 11. Correlations between the PC1 time series of omega at 500hPa in July and surface atmospheric circulation in the periods (a,c,e) 1960-2010 and (b,d,f) 2050-2100. Correlation values are estimated for a)-b) SLP (shaded and contours), c)-d) meridional wind (shaded and contours), e)-f) precipitation (shaded and contours) and vertically integrated water vapor (contours for the values -0.5, 0.3, 0.5). For a)-d) contours are shown for 0.25 and 0.5 correlation values.

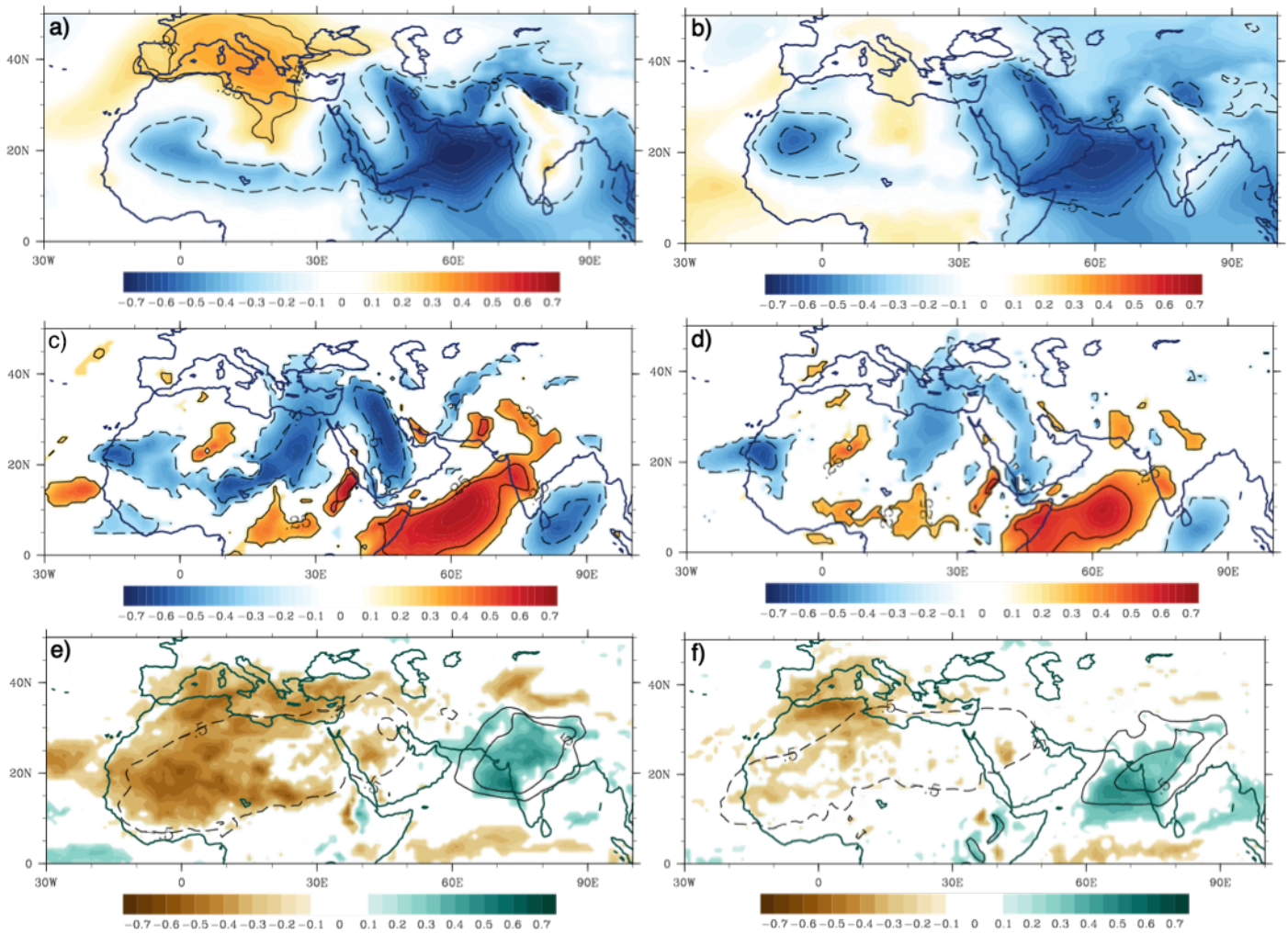

Figure 12. a) Composite differences between the sample with the 300 warmest and 300 coolest seasons over the eastern Mediterranean (30°-36°N, 36°-42°E), for July in the CTRL run, derived from a) surface temperature (°C), and associated differences in b) relative humidity, c) SLP (hPa) and vector wind at 850hpa (m/s), d) height at 850hPa (shaded) and 500hPa (contours), e) omega at 500 hPa, f) precipitation (mm/day).

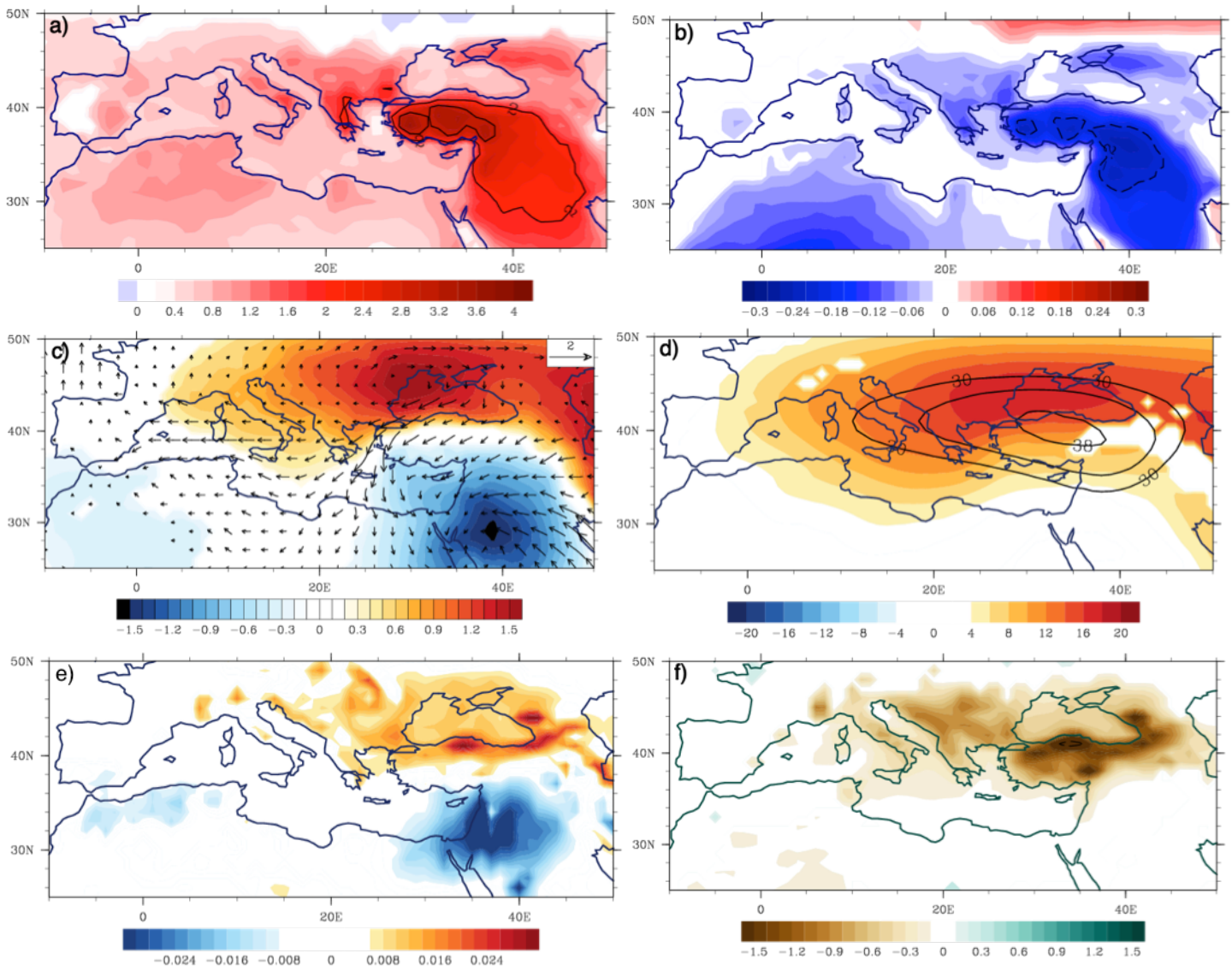

Supplementary Material

Fig SI1. Spatial pattern of SNAO, derived from the 20CR reanalysis, derived from periods: 1851-1890, 1891-1930, 1931-1970, 1971-2010.

Fig SI2. Spatial patterns of the SNAO using SLP, derived from five HIST runs in 1870-1920 (left column), and 1960-2010 (right column). The pattern is shown as correlations between time series of the first PC of SLP and SLP fields in July-August. The sign of each derived EOF is arbitrary, but here the signs were converted to match the SNAO at its negative phase.

Fig SI3. Spatial pattern of SNAO using SLP derived from the period 1970-2030 in the five HIST+PROJ runs. The pattern is shown as correlations between the principal component time series of the first EOF of SLP and SLP fields in July-August.

Figure SI4. (left) Mean storm track patterns for 1950–1990 (top) and 1970-2011 (bottom), represented by the standard deviation of daily 300 hPa geopotential height (m) in July–August. The data was bandpass-filtered on time scales of 2–8 days. (right) Correlations derived between the standard deviation of the filtered seasonal (July-August) values of 300-hPa height (derived from NCEP/NCAR 1 data) and the SNAO index (derived from 20CR data).

Fig SI5. Future changes projected for vertical velocities at a) 500 hPa, c) 600 hPa, e) 700 hPa in JJA and in July in b), d), f) respectively. The changes are derived in the period 2061-2099 and compared with the baseline period 1961-1999, derived at the original horizontal resolution (~0.25°). The vertical axis is oriented downward, i.e. negative tendencies (in blue) indicate upward motion while positive tendencies (red, stronger subsidence) indicate downward motion.

Figure SI6. Projected future changes for the summer (JJA) surface temperature (left,°C), and precipitation (right, mm/day) based on the 10-member ensemble simulations of the CSIRO-Mk3-6-0 model, for the forcing scenario RCP8.5.

Fig SI7. As in Fig 11, except that correlations are derived, based on the sample with the 300 coldest (a,b) and 300 warmest (c,d) complete seasons over the eastern Mediterranean in the CTRL run. Correlations are shown for a)-b) meridional wind, c)-d) precipitation.

Fig SI8. As in Figure 12c, except that for a) June, b) August, and for a larger domain.

Fig SI9. As in Figure 12c, except that the regions used for differentiation between warmest and coolest seasons are larger: a) 0°-40°E, 30°-36°N, b) 20°-40°E, 30°-36°N, c) 30°-50°E, 30°-36°N, d) 30°-50°E, 30°-40°N, e) 30°-50°E, 30°-45°N.

Fig SI10. Correlations between the principal component time series of EOF1 omega over EMED and precipitation in (a) June, (b) July (as in Figure 8c), (c) August. Solid lines denote positive correlations, and stippled denote negative correlations, both for the absolute values larger, than 0.25.